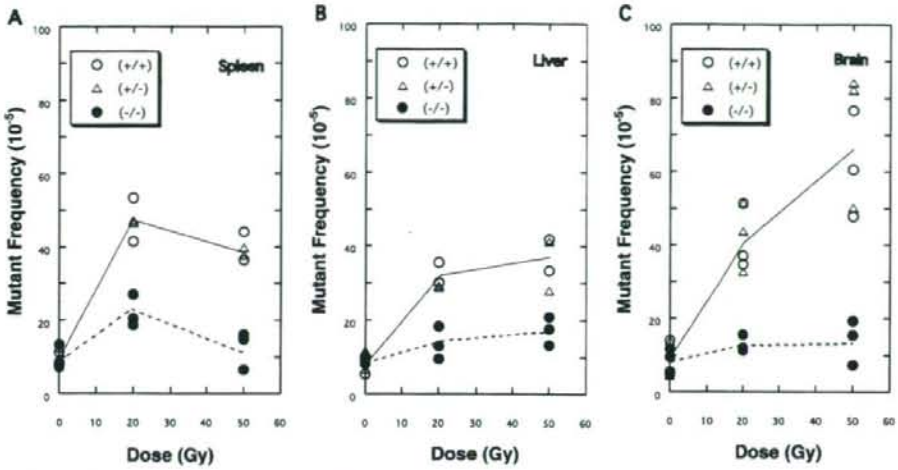

FIG. 1. Effects of *Ku70* genotype on radiation-induced *lacZ* mutations in the spleen (panel A), liver (panel B) and brain (panel C) of Muta™ mouse. Mutant frequencies after whole-body exposure to 0, 20 and 50 Gy radiation were examined in $Ku70^{+/+}$, $^{+/-}$ and $^{-/-}$ *lacZ* transgenic mice. No difference was observed between $Ku70^{+/+}$ and $^{+/-}$ mice.

ferred to nitrocellulose membranes, and analyzed for H2AX and phosphorylated H2AX (γ-H2AX) using antibodies specific for each protein; anti-H2AX Ab was made using the C terminal peptide of human H2AX as an antigen; a monoclonal Ab for γ-H2AX [Phospho-Histone H2AX (Ser139)] was purchased from Cell Signaling Technology Inc., Danvers, MA). The procedures have been described elsewhere (*32*). Non-phosphorylated and phosphorylated H2AX were compared by Western blots as an indication of the presence of DNA breaks in cells (*33*).

RESULTS

Radiation-Induced Mutations

The mutant frequencies in spleen, liver and brain after exposure to 0, 20 or 50 Gy X rays are shown in Fig. 1. $Ku70^{+/+}$ and $^{+/-}$ mice showed increased mutation frequencies after irradiation, whereas $Ku70^{-/-}$ mice showed reduced mutation levels in all three tissues compared to *Ku70*-proficient mice. $Ku70^{+/+}$ and $^{+/-}$ mice had no appreciable differences. The spontaneous levels of mutations were similar for all three genotypes. The number of mutations induced by 20 Gy were calculated by subtracting the average mutant frequency of nonirradiated mice from that of irradiated mice. The numbers of induced mutations in *Ku70*-proficient and -deficient mice were compared to determine the percentages of mutations produced through a *Ku70*-dependent NHEJ process; they were 67, 82 and 86% in spleen, liver and brain, respectively.

To understand the molecular mechanisms underlying these differences, we sequenced the *lacZ* DNA of the mutant clones. The frequencies of the different types of mutations are shown in Fig. 2. In $Ku70^{+/+}$ and $^{+/-}$ mice, the predominant type of mutation induced by radiation was a deletion, whereas this type of mutation was much less frequent in $Ku70^{-/-}$ mice. The results were similar in all three tissues we examined. This indicates that the predominant type of mutation induced by radiation at the gene sequence level, a deletion, is produced through a *Ku70*-dependent NHEJ process.

Recently, Honma *et al.* reported that the predominant mutations produced at double-strand break sites made by restriction enzyme I-*Sce*I were 1- to 50-bp-long deletions (*22*). Hence we classified the deletion mutations we found into two groups: 1–50 bp and more than 50 bp (Table 1). All of the spontaneous mutations were in the former group, whereas radiation induced deletion mutations of both sizes. In *Ku70*-proficient irradiated mice, 1–50 bp was predominant, but this was not the case in *Ku70*-deficient irradiated mice (Table 1). In other words, *Ku70* deficiency results in the suppression of small deletions of 1 to 50 bp rather than the larger deletions.

Details about the infrequent mutations classified as multiple and complex mutations in Fig. 2 are presented in Table 2. These types of mutations are observed only in irradiated mice, with the exception of one found in the unirradiated spleen of the $Ku70^{-/-}$ mouse. The complex-type mutations can be explained by the deletion of a small number of nucleotides with a simultaneous insertion of a few nucleotides at the same site. This type of mutation was reported previously in wild-type Muta™ mice (*17*) and gpt delta transgenic mice (*18*) after irradiation. The multiple mutations we encountered can be grouped into two categories: (1) two or three changes within 14 nucleotides and (2) two alterations observed separately with a distance of 558 bp or more. Interestingly, the latter class of mutation was found only in irradiated $Ku70^{-/-}$ mice (four cases) and not in unirradiated mice or irradiated *Ku70*-proficient mice. We found 188 independent mutations in irradiated *Ku70*-pro-

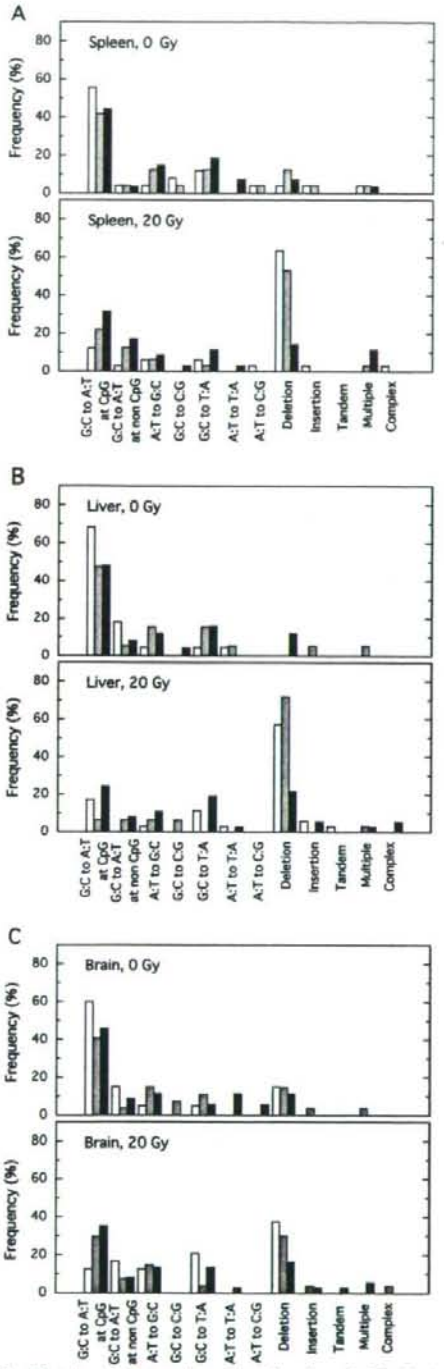

FIG. 2. Mutation spectra in nonirradiated and 20 Gy-irradiated $Ku70^{+/+}$, $^{+/-}$ and $^{-/-}$ *lacZ* transgenic mice 3.5 days postirradiation. The frequencies of different types of mutations revealed by sequencing of mutant clones are shown. Open, gray and black columns represent wild-type mice, $Ku70^{+/-}$ mice and $Ku70^{-/-}$ mice, respectively. Deletion-type mutations were induced by irradiation of $Ku70^{+/+}$ and $^{+/-}$ mice, but they were not prominent in $^{-/-}$ mice.

ficient mice and 109 in irradiated *Ku70*-deficient mice. Fisher's exact probability test showed that the number of multiple mutations appearing separately at a distance of more than 558 bp was significantly higher in $Ku70^{-/-}$ mice (4/109) than in *Ku70*-proficient mice (0/188, $P = 0.0175$).

DNA Breaks and Rejoining

The suppression of radiation-induced mutation in *Ku70*-deficient mice could be explained by lack of rejoining of DNA double-strand breaks, which would not be detected as mutations, or by repair through homologous recombination, which is known to be error-free. To obtain more information, we analyzed DNA breaks and phosphorylated H2AX, which is supposed to be associated with free ends of double-strand breaks.

SFGE was adopted to assess DNA double-strand breaks and their rejoining. With this approach, the amount of DNA breaks is estimated as the DNA released from a well into the gel after electrophoresis. The fraction of released DNA was shown to increase with radiation dose (*31*). As is indicated in Fig. 3A, immediately after exposure to 20 Gy, the amount of fragmented DNA released from the well showed an increase in all tissues of all genotypes compared to nonirradiated mice. However, 3.5 days after irradiation, the amount of fragmented DNA showed genotype- and tissue-specific differences. Fragmented DNA was much reduced in all three tissues of $Ku70^{+/-}$ mice. In $Ku70^{-/-}$ mice, on the other hand, a significant amount of DNA remained fragmented, showing suppression of DNA rejoining (Fig. 3). The statistical analysis comparing the amounts of fragmented DNAs in *Ku70*-deficient mouse tissues immediately and 3.5 days after 20 Gy irradiation showed that the rejoining was significant in liver ($P = 0.00877$) and brain ($P = 0.0104$) but not in spleen ($P = 0.0734$). This indicates that some DNA rejoining took place in the absence of *Ku70* but not as much as that observed in *Ku70*-proficient mice.

The presence of unrepaired DNA breaks in irradiated $Ku70^{-/-}$ mice was further indicated by the persistent presence of phosphorylated histone H2AX at 3.5 days postirradiation. Figure 4 shows Western blots of phosphorylated H2AX (γ-H2AX) in spleen, liver and brain at 1 h and 3.5 days after irradiation. In $Ku70^{+/-}$ mice, the γ-H2AX band observed at 1 h after irradiation disappeared at 3.5 days, whereas $Ku70^{-/-}$ mice showed significant levels of γ-H2AX at 3.5 days postirradiation, suggesting the persistent presence of unrepaired DNA breaks.

DISCUSSION

Double-strand breaks are considered to be the most important damage induced by ionizing radiation. Other types of lesions such as base damage and single-strand breaks, although more common, are repaired rapidly and do not have such disastrous consequences for cells if they are misrepaired, because they do not generally involve the loss of

TABLE 1
The Number of Deletion Mutations of Different Sizes Found in the Three Tissues

		Control			20 Gy		
Tissue	*Ku70*	Total mutations[a]	1–50 bp[b]	>50 bp[c]	Total mutations[a]	1–50 bp[b]	>50 bp[c]
Spleen	+/+, +/−	69	4 (5.8)[d]	0	64	34 (53.1)	4 (6.3)
	−/−	27	2 (7.4)	0	35	2 (5.7)	3 (8.6)
Liver	+/+, +/−	41	0	0	73	40 (54.8)	1 (1.4)
	−/−	25	3 (12.0)	0	37	5 (13.5)	3 (8.1)
Brain	+/+, +/−	47	7 (14.9)	0	51	15 (29.4)	1 (2.0)
	−/−	35	2 (5.7)	0	37	3 (8.1)	3 (8.1)

[a] Total number of independent mutations found.
[b] Number of deletion mutations of 1 to 50 bp.
[c] Number of deletion mutations of more than 50 bp.
[d] The numbers in parentheses indicate percentages.

DNA sequences from the genome. The present study demonstrates that NHEJ of DNA double-strand breaks is the major source of radiation-induced mutagenesis in mouse tissues. Double-strand breaks are only a minor component (about 1/250) of the total DNA damage (*34*). Since most of the radiation-induced mutations are suppressed in *Ku70*$^{-/-}$ mice (Fig. 1), it would appear that most DNA damage other than double-strand breaks is repaired correctly. It should be noted that a small number of mutations were induced in Ku70-deficient mice. These could be the result of mistakes in the other repair processes such as translesional DNA synthesis on damaged bases.

The number of DNA double-strand breaks induced by 1 Gy of radiation is estimated to be about 30 per cell with approximately 6×10^9 bp of total DNA (*34, 35*). The number of double-strand breaks induced in the 3.1-kbp-long *lacZ* gene by 20 Gy radiation would be estimated to be 30×10^{-5} ($30 \times 20 \times 3.1 \times 10^3/6 \times 10^9$). Since the number of radiation-induced mutations in the tissues is $23–32 \times 10^{-5}$ (Fig. 1), the two numbers are similar. This suggests that each double-strand break in the *lacZ* gene leads to one mutation. This is reasonable because most radiation-induced double-strand breaks are accompanied by chemical alterations in one or more bases or the deoxyribose at the broken ends, and they must be removed before the break is sealed. In other words, the closeness of the estimated number of DNA double-strand breaks and the measured mutant frequency suggests that the fidelity of NHEJ is very poor for radiation-induced breaks.

One point that should be remembered in the interpreta-

TABLE 2
Multiple and Complex Type Mutations

Ku70	Dose (Gy)	Tissue	ID	Type[a]	Position[b]	Change[c]	Distance between the mutations (bp)
+/+	20	Spleen	M1-12	Multiple (−3, −1)	1456–1458, 1461	A T C C T T C C C G C → A T · · · T C C · G C	3
+/−	20	Liver	M1-16	Multiple (BS, BS)	2906	C A G T C → C A T T C	14
					2921	G A T G G → G A A G G	
		Brain	F2-10	Complex (−2, +1)	2351–2352	C C G C C G → C C T C G	—
−/−	0	Spleen	F2-7	Multiple (BS, BS, BS)	1111	G T C A G → G T T A G	11, 1
					1123, 1125	A T G A G C A → A T A A A C A	
	20	Spleen	M2-12	Multiple (BS, BS)	1187	T T C G C → T T T G C	993
					2181	C G T C T → C G C C T	
			M3-16	Multiple (BS, BS)	2392	A C G A C → A C A A C	558
					2951	C G C G G → C G T G G	
			M3-17	Multiple (BS, BS)	20	T T C A C → T T T A C	116
					1187	T T C G C → T T T G C	
		Liver	M2-16	Multiple (BS, BS)	452, 454	T G G C G T T → T G T C T T T	1
			F3-13	Complex (−1, +2)	881	T C G C T → T C A T C T	—
			F3-17	Multiple (BS, BS, +1)	1369, 1370, 1372	A C C C G A G T → A C A A G A A G T	2
		Brain	M3-4	Multiple (BS, BS)	154	A T C G C → A T T G C	1041
					1196	T C C G A → T C T G A	

[a] BS; base substitution, negative number; deletion, positive number; insertion.
[b] The position of nucleotide is numbered from the first nucleotide of initiation codon of the *lacZ* gene.
[c] The nucleotides showing alteration are underlined. The deleted nucleotides are shown by dots.

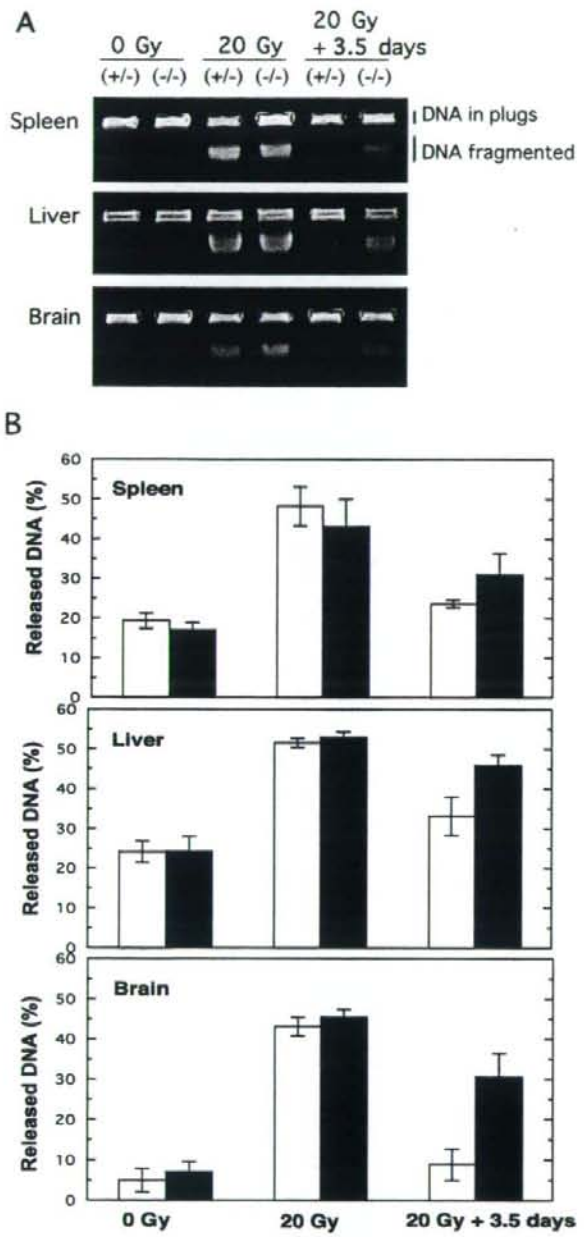

FIG. 3. SFGE analyses of DNA breaks and rejoining after 20 Gy of irradiation in *Ku70*-proficient $^{+/-}$ and deficient $^{-/-}$ mice. Panel A: Irradiation with 20 Gy increased the fraction of fragmented DNA which was released from the well in both *Ku70*$^{+/-}$ and $^{-/-}$ mice. At 3.5 days after irradiation, the fragmented DNA was reduced to the levels found in non-irradiated tissues in *Ku70*$^{+/-}$ mice and to intermediate levels in *Ku70*$^{-/-}$ mice. A similar trend was observed in the three tissues examined. Panel B: The experiment was repeated three times and the percentage of the fragmented DNA was quantified. The averages and standard deviations are shown. White columns represent *Ku70*$^{+/-}$ mice and the black columns *Ku70*$^{-/-}$ mice.

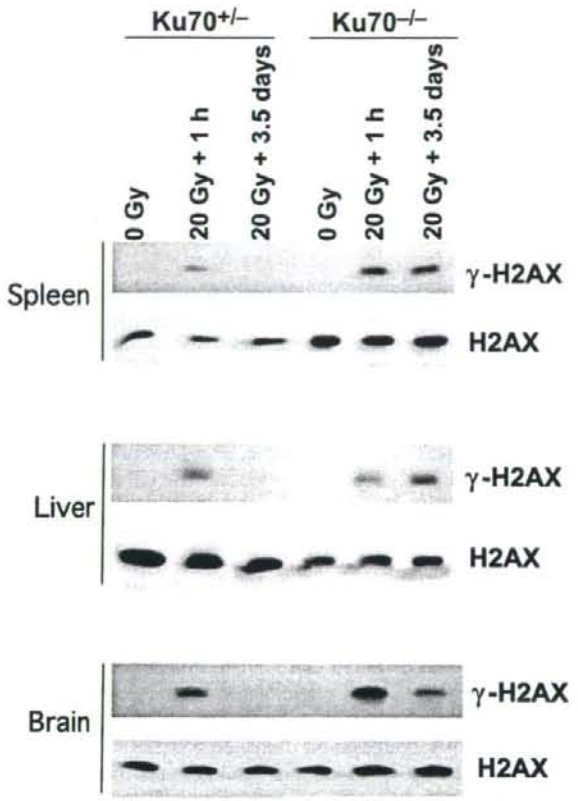

FIG. 4. Western blot analysis of the phosphorylation of histone H2AX. In *Ku70*-proficient mice, the phosphorylated H2AX (γ-H2AX) band was present at one hour after irradiation (20 Gy) and disappeared at 3.5 days in all tissues. In *Ku70*$^{-/-}$ mice, however, the γ-H2AX remained positive at 3.5 days after irradiation, suggesting that many of the radiation-induced DNA breaks remain unrepaired.

tion of the present results is that the mutational changes observed are limited to events within the 3.1-kbp-long *lacZ* gene. Therefore, large rearrangements such as deletions of more than a few kbp of DNA or translocation of the *lacZ* gene to the other chromosome cannot be detected in the present assay system, because each *lacZ* gene retrieved from the mouse genome needs to be packed into a λ phage to be analyzed for mutations. Thus the assay can monitor only base substitutions and deletions/insertions of up to a few kbp within or including the *lacZ* gene.

The other point to be noted is that the doses used in the present study are 20 Gy and 50 Gy. Although liver and brain tissue did not show any appreciable alterations after irradiation with those doses, the spleen was significantly smaller 3.5 days after irradiation. This is in accord with the prevalence of cell death in the spleen within 24 h after irradiation (*36*). Thus the data for spleen at 3.5 days after irradiation must represent the survival of only a minor fraction of spleen cells after these high doses. Further, defi-

ciency of Ku80, the other key protein of NHEJ, has been shown to enhance apoptosis in the spleen after irradiation (*36*). Thus it is possible that the reduction of radiation-induced mutations in the spleen of NHEJ-deficient mice reflects the preferential elimination of cells harboring a *lacZ* mutation. However, this is not likely, because it is difficult to imagine that the apoptosis induction system can work preferentially on cells that have damage or mutation on the *lacZ* gene. After irradiation with 20 Gy, each cell suffers significant DNA damage, including approximately 600 double-strand breaks, and no cell will be free of damage. The cells that have damage on the *lacZ* gene must have many other lesions on the other part of the genome. Under these conditions, it would be difficult to recognize selectively the cells containing damage in the *lacZ* gene. In addition, the *lacZ* gene used in the system does not have the promoter needed for transcription in mouse cells. Hence it is not expressed and could not be subject to selection by the cellular apoptosis system whether the gene is mutated or not.

Rothkamm *et al.* examined DNA ligation in cultured cells using pulsed-field gel electrophoresis and found that 50% of the double-strand breaks induced by an acute high dose of radiation (80 Gy) resulted in large DNA rearrangements, probably by ligation of illegitimate ends by NHEJ. The other 50% were ligated accurately without using the NHEJ repair system (*14*). Since the mutations monitored in the present study were small deletions of less than a few kbp within the *lacZ* gene, they must have belonged to the category considered to be "accurate ligation" in the study of Rothkamm *et al.* (*14*). At present, there is no way to estimate the ratio of mutation-free ligation and mutation-linked ligation in the "accurate ligation".

Our study as well as that of Rothkamm *et al.* (*14*) supports the existence of a functional double-strand break repair system other than NHEJ, because significant levels of DNA rejoining were observed after irradiation in NHEJ-deficient tissues and cells. It could be homologous recombination (HR) repair that functions as a form of error-free double-strand break repair when homologous DNA sequences are present. The strong repression of mutation induction in *Ku70*-deficient mouse tissues supports the importance of HR in these cells. It is also possible that microhomology-mediated end joining (MMEJ), which is error-prone and is suggested to be distinct from NHEJ (*3*), may function in NHEJ-deficient cells. Repair by MMEJ has been reported to result in relatively large deletions with short repeat sequences at the ends of deleted fragment (*3*). The frequency of repeated sequences at the ends of deleted DNA, a hallmark of MMEJ, was similar in both wild-type and *Ku70*-deficient mice (data not shown), which does not support a role for MMEJ. However, the deletion mutations observed in irradiated *Ku70*-deficient mice appear to contain slightly larger deletions than those in *Ku70*-proficient irradiated mice (Table 1), which may support the latter idea.

In the present study, we found nine multiple mutations (Table 2). Among them five cases showed two or three alterations located within a short stretch of nucleotides less than 30 bp long. This could be induced by clustered damage or by locally multiply damaged sites suggested by computer simulation of DNA damage (*37*). The other four multiple mutations displayed two base substitutions at separate positions located more than 500 bp apart. Since these were found only in irradiated *Ku70*-deficient mice, this type of mutation could be related to the NHEJ deficiency. Six out of eight base substitutions found in these multiple mutations were G:C to A:T transitions at CG sequences, a mutation type that is found most frequently in spontaneous mutations in vertebrates. Recently, Wang *et al.* proposed a phenomenon known as "mutation showers" as the cause of multiple mutations, which could occur as a result of a temporally unstable DNA polymerase or an imbalance in the deoxyribonucleotide triphosphate pool size (*38*). The multiple mutations observed in the present study could be explained by the same mechanism, although there is no evidence that Ku70 is involved in DNA polymerization or the maintenance of nucleotide pool levels.

In the present study we examined three tissues with different cell proliferation properties and asked whether there is any tissue specificity in mutation induction. The dose response of mutation induction revealed variation among the tissues, especially at 50 Gy (Fig. 1). The suppression of mutation induction at high doses could be explained by an increased probability of having two events in a single cell: mutation on the *lacZ* gene and a lethal hit for the cell. In fact, the strongest suppression was observed in the spleen, which was the most sensitive tissue among the three tissues examined. Brain cells would be more radioresistant than spleen and liver cells.

In conclusion, in *Ku70*$^{-/-}$ mice, end rejoining of X-ray-induced DNA breaks is impaired due to the absence of NHEJ repair, and the formation of mutations is suppressed. On the other hand, some non-NHEJ mediated DNA rejoining, which could be homologous recombination repair, appears to occur in *Ku70*-deficient animals.

ACKNOWLEDGMENTS

We thank Dr Frederick W. Alt for providing the *Ku70*$^{+/-}$ mice and Yasuko Syono, Yukiko Ikeda and Akemi Miura for technical support. The study was supported by grants from the "Ground-based Research Program for Space Utilization" promoted by the Japan Space Forum, the Budget for Nuclear Research of the Ministry of Education, Culture, Sports, Science and Technology, based on screening and counseling by the Atomic Energy Commission, and the NIFS Collaborative Research Program (NIFS07KOBS012).

Received: November 10, 2007; accepted: March 25, 2008

REFERENCES

1. M. R. Lieber, Y. Ma, U. Pannicke and K. Schwarz, Mechanism and regulation of human non-homologous DNA end-joining. *Nat. Rev. Mol. Cell Biol.* **4**, 712–720 (2003).

2. J. A. Downs and S. P. Jackson, A means to a DNA end: the many roles of Ku. *Nat. Rev. Mol. Cell Biol.* **5**, 367–378 (2004).
3. J. Thacker and M. Z. Zdzienicka, The XRCC genes: expanding roles in DNA double-strand break repair. *DNA Repair* **3**, 1081–1090 (2004).
4. S. Burma, B. P. C. Chen and D. J. Chen, Role of non-homologous end joining (NHEJ) in maintaining genomic integrity. *DNA Repair* **5**, 1042–1048 (2006).
5. D. Buck, L. Malivert, R. de Chasseval, A. Barraud, M-C. Fondanèche, O. Sanal, A. Plebani, J-L. Stéphan, M. Hufnagel and P. Revy, Cernunnos, a novel nonhomologous end-joining factor, is mutated in human immunodeficiency with microcephaly. *Cell* **124**, 287–299 (2006).
6. P. Ahnesorg, P. Smith and S. P. Jackson, XLF interacts with the XRCC4-DNA ligase IV complex to promote DNA nonhomologous end-joining. *Cell* **124**, 301–313 (2006).
7. A. Nijnik, L. Woodbine, C. Marchetti, S. Dawson, T. Lambe, C. Liu, N. P. Rodrigues, T. L. Crockford, E. Cabuy and R. J. Cornall, DNA repair is limiting for haematopoietic stem cells during ageing. *Nature* **447**, 686–693 (2007).
8. D. J. Rossi, D. Bryder, J. Seita, A. Nussenzweig, J. Hoeijmakers and I. L. Weissman, Deficiencies in DNA damage repair limit the function of haematopoietic stem cells with age. *Nature* **447**, 725–729 (2007).
9. Z. E. Karanjawala, U. Grawunder, C-L. Hsieh and M. R. Lieber, The nonhomologous DNA end joining pathway is important for chromosome stability in primary fibroblasts. *Curr. Biol.* **9**, 1501–1506 (1999).
10. D. O. Ferguson, J. M. Sekiguchi, S. Chang, K. M. Frank, Y. Gao, R. A. DePinho and F. W. Alt, The nonhomologous end-joining pathway of DNA repair is required for genomic stability and the suppression of translocations. *Proc. Natl. Acad. Sci. USA* **97**, 6630–6633 (2000).
11. M. J. Difillppantonlo, J. Zhu, H. T. Chen, E. Meffre, M. C. Nussenwig, E. E. Max, T. Ried and A. Nussenzweig, DNA repair protein Ku80 suppresses chromosomal aberrations and malignant transformation. *Nature* **404**, 510–514 (2000).
12. L. D. Rockwood, A. Nussenzweig and S. Janz, Paradoxical decrease in mutant frequencies and chromosomal rearrangements in a transgenic *lacZ* reporter gene in Ku80 null mice deficient in DNA double strand break repair. *Mutat. Res.* **529**, 51–58 (2003).
13. M. Martín, A. Genescà, L. Latre, I. Jaco, G. E. Taccioli, J. Egozcue, M. A. Blasco, G. Iliakis and L. Tusell, Postreplicative joining of DNA double-strand breaks causes genomic instability in DNA-PKcs-deficient mouse. *Cancer Res.* **65**, 10223–10232 (2005).
14. K. Rothkamm, M. Kühne, P. A. Jeggo and M. Löbrich, Radiation-induced genomic rearrangements formed by nonhomologous end-joining of DNA double-strand breaks. *Cancer Res.* **61**, 3886–3893 (2001).
15. Y. Peng, Q. Zhang, H. Nagasawa, R. Okayasu, H. L. Liber and J. S. Bedford, Silencing expression of the catalytic subunit of DNA-dependent protein kinase by small interfering RNA sensitizes human cells for radiation-induced chromosome damage, cell killing, and mutation. *Cancer Res.* **62**, 6400–6404 (2002).
16. T. Zhou and L. F. Povirk, Extreme cytotoxicity and susceptibility to hprt mutagenesis in Ku-deficient xrs-6 cells treated with bleomycin in plateau phase. *Mutagenesis* **20**, 39–44 (2005).
17. T. Ono, H. Ikehata, S. Nakamura, Y. Saito, J. Komura, Y. Hosoi and K. Yamamoto, Molecular nature of mutations induced by a high dose of X-rays in spleen, liver, and brain of the *lacZ*-transgenic mouse. *Environ. Mol. Mutagen.* **34**, 97–105 (1999).
18. K. Masumura, K. Kuniya, T. Kurobe, M. Fukuoka, F. Yatagai and T. Nohmi, Heavy-ion-induced mutations in the gpt delta transgenic mouse: comparison of mutation spectra induced by heavy-ion, X-ray, and γ-ray radiation. *Environ. Mol. Mutagen.* **40**, 207–215 (2002).
19. Y. Gu, S. Jin, Y. Gao, D. T. Weaver and F. W. Alt, Ku70-deficient embryonic stem cells have increased ionizing radiosensitivity, defective DNA end-binding activity, and inability to support V(D)J recombination. *Proc. Natl. Acad. Sci. USA* **94**, 8076–8081 (1997).
20. F. Liang, M. Han, P. J. Romanienko and M. Jasin, Homology-directed repair is a major double-strand break repair pathway in mammalian cells. *Proc. Natl. Acad. Sci. USA* **95**, 5172–5177 (1998).
21. M. Honma, M. Izumi, M. Sakuraba, S. Tadokoro, H. Sakamoto, W. Wang, F. Yatagai and M. Hayashi, Deletion, rearrangement, and gene conversion; genetic consequences of chromosomal double-strand breaks in human cells. *Environ. Mol. Mutagen.* **42**, 288–298 (2003).
22. M. Honma, M. Sakuraba, T. Koizumi, Y. Takashima, H. Sakamoto and M. Hayashi, Non-homologous end-joining for repairing I-SceI-induced DNA double strand breaks in human cells. *DNA Repair* **6**, 781–788 (2007).
23. M. E. T. Dollé, W. K. Snyder, J. A. Gossen, P. H. M. Lohman and J. Vijg, Distinct spectra of somatic mutations accumulated with age in mouse heart and small intestine. *Proc. Natl. Acad. Sci. USA* **97**, 8403–8408 (2000).
24. T. Ono, H. Ikehata, V. P. Pithani, Y. Uehara, Y. Chen, Y. Kinouchi, T. Shimosegawa and Y. Hosoi, Spontaneous mutations in digestive tract of old mice show tissue-specific patterns of genomic instability. *Cancer Res.* **64**, 6919–6923 (2004).
25. T. Ono, H. Ikehata, Y. Uehara and J. Komura, The maintenance of genome integrity is tissue-specific. *Genes Environ.* **28**, 16–22 (2006).
26. K. E. Orii, Y. Lee, N. Kondo and P. J. McKinnon, Selective utilization of nonhomologous end-joining and homologous recombination DNA repair pathways during nervous system development. *Proc. Natl. Acad. Sci. USA* **103**, 10017–10022 (2006).
27. L. Brugmans, R. Kanaar and J. Essers, Analysis of DNA double-strand break repair pathways in mice. *Mutat. Res.* **614**, 95–108 (2007).
28. J. A. Gossen, W. J. F. de Leeuw, C. H. T. Tan, E. C. Zwarthoff, F. Berends, P. H. M. Lohman, D. L. Knook and J. Vijg, Efficient rescue of integrated shuttle vectors from transgenic mice: a model for studying mutations *in vivo*. *Proc. Natl. Acad. Sci. USA* **86**, 7971–7975 (1989).
29. Y. Gu, K. J. Seidl, G. A. Rathbun, C. Zhu, J. P. Manis, N. van der Stoep, L. Davidson, H-L. Cheng and F. W. Alt, Growth retardation and leaky SCID phenotype of Ku70-deficient mice. *Immunity* **7**, 653–665 (1997).
30. F. Wang, Y. Saito, T. Shiomi, S. Yamada, T. Ono and H. Ikehata, Mutation spectrum in UVB-exposed skin epidermis of a mildly-affected Xpg-deficient mouse. *Environ. Mol. Mutagen.* **47**, 107–116 (2006).
31. R. Hirayama, Y. Furusawa, T. Fukawa and K. Ando, Repair kinetics of DNA-DSB induced by X-rays or carbon ions under oxic and hypoxic conditions. *J. Radiat. Res.* **46**, 325–332 (2005).
32. J. Sambrook and D. W. Russell, SDS-polyacrylamide gel electrophoresis of proteins. *In Molecular Cloning- A Laboratory Manual*, 3rd ed. (J. Sambrook and D. W. Russell, Eds.), pp. A8.40–A8.55. Cold Spring Harbor Laboratory Press, Cold Spring Harbor, NY, 2001.
33. K. Rothkamm and M. Löbrich, Evidence for a lack of DNA double-strand break repair in human cells exposed to very low x-ray doses. *Proc. Natl. Acad. Sci. USA* **100**, 5057–5062 (2003).
34. J. F. Ward, DNA damage produced by ionizing radiation in mammalian cells: identities, mechanisms of formation, and reparability. *Prog. Nucleic Acids Res. Mol. Biol.* **35**, 95–125 (1988).
35. B. Stenerlöw, K. H. Karlsson, B. Cooper and B. Rydberg, Measurement of prompt DNA double-strand breaks in mammalian cells without including heat-labile sites: Results for cells deficient in nonhomologous end joining. *Radiat. Res.* **159**, 502–510 (2003).
36. A. Nussenzweig, K. Sokol, P. Burgman, L. Li and G. C. Li, Hypersensitivity of *Ku80*-deficient cell lines and mice to DNA damage: The effects of ionizing radiation on growth, survival, and development. *Proc. Natl. Acad. Sci. USA* **94**, 13588–13593 (1997).
37. H. Nikjoo, P. O'Neill, D. T. Goodhead and M. Terrissol, Computational modelling of low-energy electron-induced DNA damage by early physical and chemical events. *Int. J. Radiat. Biol.* **71**, 467–483 (1997).
38. J. Wang, K. D. Gonzalez, W. A. Scaringe, K. Tsai, N. Liu, D. Gu, W. Li, K. A. Hill and S. S. Sommer, Evidence for mutation showers. *Proc. Natl. Acad. Sci. USA* **104**, 8403–8408 (2007).

H., Poeck, H., Akira, S., Conzelmann, K.K., Schlee, M., Endres, S., & Hartmann, G. (2006) *Science*, 314, 994–997.
8) Pichlmair, A., Schulz, O., Tan, C.P., Naslund, T.I., Liljestrom, P., Weber, F., & Reis e Sousa, C. (2006) *Science*, 314, 997–1001.
9) Kato, H., Takeuchi, O., Mikano-Satoh, E., Hirai, R., Kawai, T., Matsushita, K., Hiiragi, A., Dermody, T.S., Fujita, T., & Akira, S. (2008) *J. Exp. Med.*, 205, 1601–1610.
10) Takahasi, K., Yoneyama, M., Nishihori, T., Hirai, R., Kumeta, H., Narita, R., Gale, M., Jr., Inagaki, F., & Fujita, T. (2008) *Mol. Cell*, 29, 428–440.
11) Cui, S., Eisenacher, K., Kirchhofer, A., Brzozka, K., Lammens, A., Lammens, K., Fujita, T., Conzelmann, K.K., Krug, A., & Hopfner, K.P. (2008) *Mol. Cell*, 29, 169–179.

米山 光俊[1,2]，藤田 尚志[1]
([1]京都大学ウイルス研究所・分子遺伝学研究分野，
[2]科学技術振興機構さきがけ研究員)

Non-self RNA-sensing mechanism of RIG-I RNA helicase
Mitsutoshi Yoneyama[1,2] and Takashi Fujita[1] ([1]Laboratory of Molecular Genetics, Institute for Virus Research, Kyoto University, 53 Shogoinkawahara-cho, Sakyo-ku, Kyoto 606–8507, Japan; [2]PRESTO, Japan Science and Technology Agency, 4–1–8 Honcho Kawaguchi, Saitama 332–0012, Japan)

誘発突然変異と損傷乗り越えDNA合成 —REV1の構造と生化学的機能—

1. はじめに

誘発突然変異は，電離放射線や紫外線，化学物質などの変異誘発剤によって誘発される突然変異を指す．変異誘発剤はWatson-Crick型の塩基対合を変化させるようなDNA損傷を引き起こすが，突然変異が誘発されるためには，DNA損傷に加えて細胞内の積極的な機能が必要不可欠である．*REV1*遺伝子（reversionless）は，この突然変異誘発に必要不可欠な酵母の遺伝子として同定された．本稿では，酵母及びヒトREV1の構造と生化学的特性から突然変異誘発における機能を概説する．

2. 誘発突然変異と損傷乗り越えDNA合成

細胞に紫外線が照射されると，新生DNA鎖の断片化が観察される．これは，複製型のDNAポリメラーゼ（pol δまたはpol ε）が，紫外線損傷に対してDNA伸長反応を停止することに起因する．その後，この断片化したDNAはより大きなDNAに移行するが，この過程を複製後修復（post-replication repair）と呼ぶ．複製後修復では，損傷塩基は除去せずに，断片化したDNAどうしを繋げることにより，複製過程で生じたギャップを修復する[1,2]．

酵母では，*RAD*（radiation sensitivity）遺伝子群として同定された遺伝子の中で，複製後修復に関与する遺伝子群は*RAD6*エピスタシス群として分類される．複製後修復経路は，ユビキチンリガーゼE2-E3であるRAD6-RAD18複合体によるproliferating cell nuclear antigen（PCNA）のモノユビキチン化により制御される．損傷乗り越えDNA合成（translesion DNA synthesis, TLS）経路はRAD6-RAD18の下流で機能する複製後修復経路の一つである．TLS経路では，特殊なDNAポリメラーゼ（TLSポリメラーゼ）が，損傷塩基を鋳型としたDNA合成反応により，DNA複製を回復する[1,2]．

酵母の*REV1*遺伝子は，紫外線による突然変異の誘発が抑制される変異体として同定された．*rev1*株では，紫外線や電離放射線をはじめ，様々な種類の薬剤による突然変異の誘発が抑制され，同時にそれら薬剤に対する感受性が増大する[3]．Lawrenceのグループは1996年に酵母のREV1タンパク質がDNA損傷の一つ，脱塩基部位（DNA上の塩基が脱離しデオキシリボースだけになった状態のDNA損傷）に対して，dCMPを対合するデオキシシチジルトランスフェラーゼであることを発見した[4]．

一方，色素性乾皮症バリアント群（XP-V）に分類される患者由来の細胞では，紫外線による誘発突然変異頻度が高いこと，紫外線照射後の複製後修復に欠損のあることが知られていた[2]．花岡のグループは1999年にXP-Vの責任遺伝子がシクロブタン型チミンダイマーに対してdAMPを対合する活性をもつpol ηをコードすることを明らかにした[5]．TLS経路で機能するこれらの酵素は構造的に類似しており，Y-ファミリーのDNAポリメラーゼとして分類されている[6]．XP-Vの患者由来の細胞ではpol ηの代わりに，別のTLSポリメラーゼが働き，dAMP以外の塩基を挿入した結果，突然変異頻度が上昇すると考えられている[2]．

Y-ファミリーのDNAポリメラーゼは，原核生物から高等真核生物まで広く保存されており，ヒトではpol η，pol ι，pol κ，REV1の4種類が存在する（図1）[6]．REV1はY-ファミリーのメンバーではあるが，その活性はdCMP転移活性に限られ，他の基質dATP，dGTP，dTTPに対する親和性は極めて低く，実質上ポリメラーゼ活性はない．真核生物のポリメラーゼでは，触媒ドメイン以外にも多くの類似

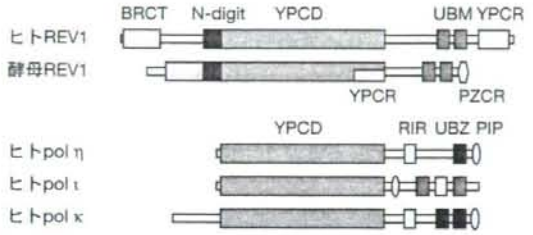

図1 Y-ファミリーDNAポリメラーゼの構造

BRCT: BRCA1 C-terminus domain, YPCD: Y-family DNA polymerase catalytic domain, YPCR; Y-family DNA polymerase contacting region, PZCR: polymerase ζ contacting region, UBM: ubiquitin binding motif, UBZ: ubiquitin binding Zn finger, PIP: PCNA interacting protein box, RIR: REV1 interacting region.

点がある（図1）[6]．ユビキチン結合ドメイン（UBMまたはUBZ），PCNAと結合する配列（PIP box）は，Y-ファミリーのポリメラーゼが損傷部位で機能する際，ユビキチン化されたPCNAと相互作用するために必要であると考えられている．また，全てのポリメラーゼにはREV1と相互作用する領域が同定されているが，この相互作用の意義は今のところ不明である．

3. TLS酵素としてのREV1の構造と機能

REV1のdCMP転移活性は，鋳型Gに対する効率が最も高いが，損傷部位としては脱塩基部位に対して効率よくdCMPを対合する[4,7]．REV1がdCTPを認識する分子機構はとてもユニークである．REV1は触媒ドメインのN末端側にREV1に特徴的なドメイン（N-digit）をもち，この中のアルギニン残基がシトシンとの水素結合によりdCTPを認識する．一方，鋳型Gは外側に追い出され，空いた間隙はアルギニン残基に隣接するロイシン酸残基により占められる[6]．脱塩基部位に対する結合もこのロイシン残基により安定化されるものと思われる．生体内では，DNA上のあらゆる塩基が脱離することによって脱塩基部位が生じると考えられ，脱塩基部位に対するdCMPの取り込みは，塩基置換の原因となりうる[3]．REV1はdCTPの選択性に関してとても巧妙な構造をもつが，なぜ取り込まれる塩基がdCMPであるのか，その生物学的理由は明らかでない．

REV1のdCMP転移活性が，細胞内でTLSに機能しているという証拠は，酵母を使った研究から示されている．Dempleのグループは，チミンまたはシトシン塩基をDNAから除去する活性を獲得した変異型DNAグリコシラーゼを酵母で発現させ，生じた脱塩基部位に挿入される塩基を解析した[8]．その結果，どちらのグリコシラーゼを発現させた場合にも突然変異頻度が上昇し，その大部分にREV1依存的なdCMPの挿入が観察された．

4. REV1の第二の機能と構造

酵母では*REV1*遺伝子が欠損すると様々なDNA損傷に対して感受性となると同時に，突然変異の誘発が抑制される．実際に，T-T（6-4）光産物を含むプラスミドを酵母に導入しその TLS を解析すると，約7割のケースでdAMPの取り込みによる正しいTLSが観察され，3割のケースでdTMPまたはdGMPの挿入による誤ったTLSが観察される．興味深いことに，どちらのTLSも*REV1*依存的であるにもかかわらず，dCMPの挿入が観察されない．さらに，このTLSにはREV1の触媒活性は必要なく，むしろBRCTドメインが必要であることから，REV1の第二の機能と呼ばれている[3]．REV1が関与する多くのTLSと突然変異誘発は，この第二の機能が関わっている．

酵母の遺伝学的解析では，*REV1*は他の*REV*遺伝子，*REV3*，*REV7*とエピスタティックである．したがって，突然変異誘発におけるREV1の機能（REV1の第二の機能）はREV3，REV7と同一の生化学的過程にあると予想される[3]．*REV3*はpol ζの触媒サブユニット，*REV7*は非触媒サブユニットをコードし，安定な複合体pol ζを構成する．pol ζはY-ファミリーのTLSポリメラーゼとは構造的に異なったもう一つのTLSポリメラーゼである[3]．酵母のREV1では，pol ζと相互作用する部位が同定され（図1），REV1によるpol ζの活性促進が観察される．また，その領域を欠失したREV1では紫外線感受性を示すと同時に，突然変異の誘発が見られないことから，REV1の第二の機能のある部分は，この相互作用を介したpol ζの活性促進によるものであると考えられる[9]．しかしヒトにおいては，REV1とpol ζとの相互作用は明らかになっていない．

REV1に特徴的なもう一つの構造として，他のY-ファミリーのポリメラーゼと相互作用する領域が同定されている（図1）[6]．この領域は，REV7と結合することによりREV1-REV7複合体の構成にも必要とされる[10,11]．不思議なことにREV7はREV1のdCMP転移活性に全く影響を与えない[11]．また，REV7の結合はREV1と他のY-ファミリーポリメラーゼとの相互作用を阻害する[6]．これらの結果は，TLSにおけるポリメラーゼの選択等の調節にREV7が関与することを示唆するのかもしれない．

REV1は他のポリメラーゼとは異なり，PCNAと相互作用するPIP boxが見いだされない．実際に，酵母REV1はPCNAにより活性化されないという報告があり[12]，我々も

ヒトREV1で同様の結果を得ている．一方で，PCNAが酵母REV1のC末端側と相互作用し，活性化するという報告もある[13]．この活性化は，ユビキチン化されたPCNAによりさらに促進され，REV1のUBMに依存する．この結果は酵母の遺伝学によっても支持され，UBMを欠失した*rev1*では紫外線感受性を示すと同時に突然変異が誘発されない．一方これらの結果に反して，マウスRev1ではBRCTドメインがPCNAと相互作用するとの報告もあり[14]，これらの矛盾が解決されるためにはさらなる解析が必要である．

5. REV1の単鎖DNA結合活性

我々は，REV1が単鎖DNA結合活性をもつことを見いだした[15]．この活性がREV1のdCMP転移反応にどのように作用するかを調べるために，長さの違う3種類のプライマーテンプレートを作成した（図2Aa–c下段）．これらのプライマーテンプレートとREV1を反応させると全て同等にdCMPが重合された（図2Aa–c）．また，短い鋳型からなる二つのプライマーテンプレートを同時に反応させるとREV1は両方のプライマー末端に同様にdCMPを重合した（図2Ad）．ところが長い鋳型と短い鋳型からなるプライマーテンプレートを同時に反応させると，長い鋳型からなるプライマーに選択的に反応が観察された（図2Ae）これらの結果は，単鎖DNAに結合したREV1はその単鎖DNA上にあるプライマー末端に選択的にターゲティングされることを示しており，この過程でREV1は単鎖DNA上をスライディングしていると思われる．この性質は欠失型REV1（M5）で消失し（図2BC），polηでは観察されないことから[15]，REV1特異的である．これらの結果は，REV1の最初のターゲットが単鎖DNAである可能性を示唆する[15]．

おわりに

REV1の構造とその生化学的特性は酵母からヒトまでとてもよく保存されていることが明らかとなった．REV1は様々なタンパク質と相互作用し，Y-ファミリーのメンバーの中では，構造的，機能的に特殊な存在である．これらの相互作用は，TLSを制御するためのものであると考えられる．しかし，これまでに報告されている実験結果は依然断片的であり，REV1と突然変異誘発機構の全体像解明にはさらなる研究が必要である．

1) Andersen, P.L., Xu, F., & Xiao, W. (2008) *Cell Res.*, 18, 162–173.
2) Lehmann, A.R., Niimi, A., Ogi, T., Brown, S., Sabbioneda, S., Wing, J.F., Kannouche, P.L., & Green, C.M. (2007) *DNA Repair (Amst.)*, 6, 891–899.
3) Lawrence, C.W. (2002) *DNA Repair (Amst.)*, 1, 425–435.
4) Nelson, J.R., Lawrence, C.W., & Hinkle, D.C. (1996) *Nature*, 382, 729–731.
5) Masutani, C., Kusumoto, R., Yamada, A., Dohmae, N., Yokoi, M., Yuasa, M., Araki, M., Iwai, S., Takio, K., & Hanaoka, F.

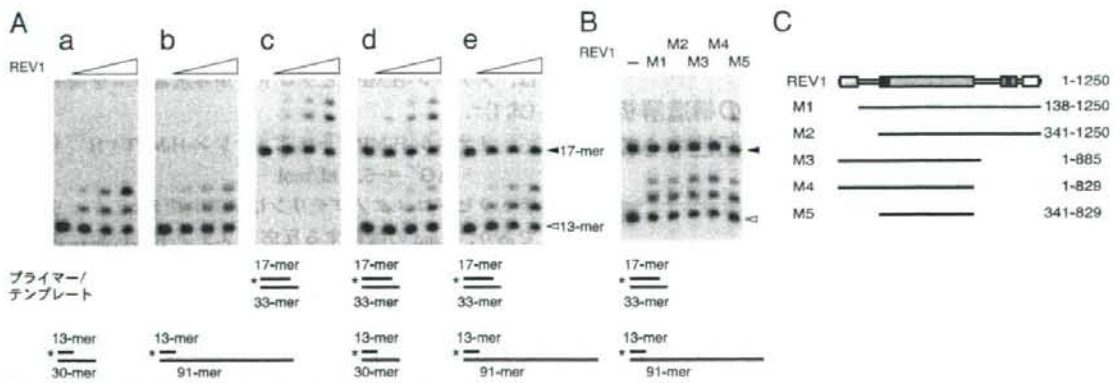

図2 単鎖DNAを介したREV1のターゲティング
A．REV1のdCMP転移反応における選択的反応性．^{32}Pで標識した（*）様々な長さのプライマーテンプレート（下段に記載）とREV1を反応させた．
B．欠失型REV1のdCMP転移反応における選択的反応性．下段に示したプライマーテンプレートと欠失型REV1を反応させた．反応産物は変性アクリルアミドゲル電気泳動後，オートラジオグラムにより解析した．
C．欠失型REV1の構造．

(1999) *Nature*, 399, 700-704.
6) Yang, W. & Woodgate, R. (2007) *Proc. Natl. Acad. Sci. USA*, 104, 15591-15598.
7) Masuda, Y. & Kamiya, K. (2002) *FEBS Lett.*, 520, 88-92.
8) Auerbach, P., Bennett, R.A., Bailey, E.A., Krokan, H.E., & Demple, B. (2005) *Proc. Natl. Acad. Sci. U S A*, 102, 17711-17716.
9) Acharya, N., Johnson, R.E., Prakash, S., & Prakash, L. (2006) *Mol. Cell. Biol.*, 26, 9555-9563.
10) Murakumo, Y., Roth, T., Ishii, H., Rasio, D., Numata, S., Croce, C.M., & Fishel, R. (2000) *J. Biol. Chem.*, 275, 4391-4397.
11) Masuda, Y., Ohmae, M., Masuda, K., & Kamiya, K. (2003) *J. Biol. Chem.*, 278, 12356-12360.
12) Haracska, L., Unk, I., Prakash, L., & Prakash, S. (2006) *Proc. Natl. Acad. Sci. U S A*, 103, 6477-6482.
13) Wood, A., Garg, P., & Burgers, P.M. (2007) *J. Biol. Chem.*, 282, 20256-20263.
14) Guo, C., Sonoda, E., Tang, T.S., Parker, J.L., Bielen, A.B., Takeda, S., Ulrich, H.D., & Friedberg, E.C. (2006) *Mol. Cell*, 23, 265-271.
15) Masuda, Y. & Kamiya, K. (2006) *J. Biol. Chem.*, 281, 24314-24321.

増田 雄司，神谷 研二
(広島大学原爆放射線医科学研究所
分子発がん制御研究分野)

Induced mutagenesis and translesion DNA synthesis—structure and function of REV1—
Yuji Masuda and Kenji Kamiya (Department of Experimental Oncology, Research Institute for Radiation Biology and Medicine, Hiroshima University, Minami-ku, Hiroshima 734-8553, Japan)

[Fe]-ヒドロゲナーゼ（Hmd）の構造解析から見えてきたヒドロゲナーゼ活性中心の収斂進化

はじめに

ヒドロゲナーゼは水素ガス（H_2）を活性化し，ヒドリドとプロトンに分解する反応を触媒する酵素である．多くのヒドロゲナーゼはヒドリドをさらに分解し，二つの電子とプロトンにする．その触媒反応は可逆であり，逆反応ではH_2が生産される[1]．ヒドロゲナーゼのバイオテクノロジーへの応用として，燃料電池電極や水素生産の触媒としての活用が注目されている[2]．

自然界において，ヒドロゲナーゼは微生物生態系の水素代謝で重要な役割を担っている．嫌気条件下，有機物は細菌や原生動物などによって分解され，有機酸やH_2になる．ここで大量のH_2が発生するが（～10^8トン/年）[3]，H_2はメタンや酢酸の生産および硫酸塩の還元に使われるため，環境中に存在するH_2濃度は低く保たれている．一部のH_2は好気環境に分散し，そこで好気性細菌によって酸化される[4]．ヒドロゲナーゼはこれらの水素代謝系で，H_2の生産と酸化を触媒する．

ヒドロゲナーゼはおよそ80年前に発見され，これまでに［NiFe］ヒドロゲナーゼと［FeFe］ヒドロゲナーゼという2種類がよく研究されてきた．名称からも明らかなように，活性中心に含まれる金属の種類が異なり，前者はニッケルと鉄を，後者は2原子の鉄を含んでいる（**図1**）[5-7]．20年ほど前，メタン菌から新しいタイプのヒドロゲナーゼが発見された．この新規酵素はひとつの鉄のみを活性中心に含んでいることから，［Fe］ヒドロゲナーゼ（Hmd）と呼ばれている（図1）[4]．

本稿では，Hmdの活性中心に関する知見を概説した後，ヒドロゲナーゼの特徴的な鉄錯体構造から，3種類のヒドロゲナーゼの進化について述べる．

1. ［Fe］-ヒドロゲナーゼ（Hmd）の機能と性質

［Fe］ヒドロゲナーゼの分類名はH_2-forming methylenetetrahydromethanopterin dehydrogenaseで，略称はHmdである．その触媒反応では，H_2を活性化してヒドリドとプロトンに分解し，ヒドリドをメテニルテトラヒドロメタノプテリン（メテニル-H_4MPT$^+$）に転移し，メチレンテトラヒドロメタノプテリン（メチレン-H_4MPT）をつくる．逆反応では，メチレン-H_4MPTとプロトンから水素ガスを発生する（式1）[4]．

$$\text{メテニル-}H_4\text{MPT}^+ + H_2 \rightleftarrows \text{メチレン-}H_4\text{MPT} + H^+ \quad (\text{式}1)$$
$$\Delta G^{\prime} = -5.5\ \text{kJ/mol}$$

テトラヒドロメタノプテリンはメタン菌のC1キャリヤーであり，Hmdの触媒する反応はメタン生成代謝に含まれる．Hmdは水素利用性のメタン菌のいくつかに見出されているが，*Methanothermobacter marburgensis*由来の酵素がよく研究されている．このメタン菌では，培地中のニッケルが制限された条件（50nM以下）でHmdが大量に生産され，全タンパク質の5%を超えることが知られている[8]．

Hmdは分子量38,000のサブユニットのホモ二量体からなり，2分子の鉄コファクター（FeGPコファクター）を含んでいる．FeGPコファクターはピリジノール環がGMP

Published online 3 October 2008

Nucleic Acids Research, 2008, Vol. 36, No. 19 ***6295–6308***
doi:10.1093/nar/gkn609

Biochemical analysis of human PIF1 helicase and functions of its N-terminal domain

Yongqing Gu[1,2], Yuji Masuda[1] and Kenji Kamiya[1,*]

[1]Research Institute for Radiation Biology and Medicine, Hiroshima University, Hiroshima 734-8553, Japan and [2]School of Medicine, Shihezi University, Shihezi, Xinjiang 832002, China

Received May 1, 2008; Revised September 8, 2008; Accepted September 9, 2008

ABSTRACT

The evolutionary conserved PIF1 DNA helicase family appears to have largely nonoverlapping cellular functions. To better understand the functions of human PIF1, we investigated biochemical properties of this protein. Analysis of single-stranded (ss) DNA-dependent ATPase activity revealed nonstructural ssDNA to greatly stimulate ATPase activity due to a high affinity for PIF1, even though PIF1 preferentially unwinds forked substrates. This suggests that PIF1 needs a ssDNA region for loading and a forked structure for translocation entrance into a double strand region. Deletion analysis demonstrated novel functions of a unique N-terminal portion, named the PIF1 N-terminal (PINT) domain. When the PINT domain was truncated, apparent affinity for ssDNA and unwinding activity were much reduced, even though the maximum velocity of ATPase activity and K_m value for ATP were not affected. We suggest that the PINT domain contributes to enhancing the interaction with ssDNA through intrinsic binding activity. In addition, we found DNA strand-annealing activity, also residing in the PINT domain. Notably, the unwinding and annealing activities were inhibited by replication protein A. These results suggest that the functions of PIF1 might be restricted with particular situations and DNA structures.

INTRODUCTION

Helicases are ubiquitous enzymes that catalyze the unwinding of DNA duplexes using ATP as their energy source. They therefore play vital roles in nearly all DNA metabolic processes, including DNA replication, recombination and repair. The PIF1 subfamily of 5′–3′ DNA helicases (1–10) belongs to the SFI superfamily, conserved in diverse organisms (11).

In *Saccharomyces cerevisiae* (*Sc*), *Sc*Pif1 was originally identified because of its involvement in recombination of mitochondrial DNA (mtDNA) (12,13). Dysfunction of *Sc*Pif1 leads to mitochondrial genetic instability due to spontaneous oxidative damage (14–16), and induces mtDNA damage (17). *Sc*Pif1p has not only mitochondrial targeting but also nuclear targeting signals and therefore is localized in both the mitochondria and nucleus (18). Nuclear *Sc*Pif1p has multiple functions. When it is overproduced, telomeres become shorter, while they elongate when it is eliminated (18,19). In the absence of nuclear *Sc*Pif1, gross chromosome rearrangement is also increased, and healing of double-stranded broken ends via telomere addition increases ~200- to 1000-fold. These data suggest a negative regulatory role of *Sc*Pif1 in telomere metabolism (18–24). Indeed, *Sc*Pif1 catalytically inhibits telomerase activity *in vitro* (25). Other genetic data suggest that *Sc*Pif1 plays roles in Okazaki fragment processing (26), pausing of replication progression at ribosomal DNA loci (27) and unwinding of hemicatenans (28).

Schizosaccharomyces pombe encodes a PIF1 homolog, Pfh1 (8,10) which is required for cell cycle progression in late *S*-phase and for appropriate responses to DNA damage agents (8,10). It is also implicated in lagging strand DNA processing (7).

Previous biochemical studies of human PIF1 were performed using N-terminal-truncated forms of PIF1, containing only the conserved helicase motifs, located in the C-terminus, since it earlier proved impossible to obtain purified full-length human PIF1 protein (3,4,9). However, we found that the N-terminal region of human PIF1, named here as the PIF1 N-terminal (PINT) domain, is well conserved in the PIF1 family, suggesting a possible functional role. Here, we established a method to purify full-length human PIF1 protein and provided the first evidence that the PINT domain has crucial functions in this enzyme.

MATERIALS AND METHODS

Plasmid construction

The nucleotide sequence of the 5′-end of human PIF1 cDNA was obtained by 5′-rapid amplification of cDNA ends. Then the full-length human *PIF1* cDNA was

*To whom correspondence should be addressed. Tel: +81 82 257 5842; Fax: +81 82 257 5844; Email: kkamiya@hiroshima-u.ac.jp

amplified from a HeLa cDNA library using primers, CATATGCTCTCGGGCATAGAGGCGGCGGCAGG GGAATATGAGGACTCG and TCAGAGGATTGGG TCCATGTT by PCR, then the nucleotide sequences of the clones were verified and submitted to the database with the accession number, EU084033. The entire coding region with a histidine tag at the N-terminus was inserted into the pET20b(+) vector to yield pET20b-PIF1. The truncated forms, $PIF^{167-641}$ and PIF^{1-180} consisting of the numbered amino acid residues were also cloned into pET20b(+) and pET15b, respectively, to produce his-tagged fusion proteins. The structures of the resultant plasmids, pET20b-PIF1, pET20b-$PIF^{167-641}$ and pET15b-PIF^{1-180}, are shown in Supplementary Figure S1. In this article, $PIF^{167-641}$ and PIF^{1-180} are referred to as C-terminal region of PIF1 (PIF1C) and N-terminal region of PIF1 (PIF1N), respectively.

Protein purification

RPA was purified as described (29) from over producing *Escherichia coli* cells (30). PIF1 and its deletion derivatives were purified as his-tagged fusion proteins at the N-termini. During all the purification steps, induced proteins were monitored by SDS–PAGE followed by staining with Coomassie Brilliant Blue R-250, or western blotting using Penta-His antibody (#34660, QIAGEN, Tokyo, Japan) or anti-PIF1 antibodies. Protein concentrations were determined by Bio-Rad protein assay using BSA (Bio-Rad, Tokyo, Japan) as the standard.

His-tagged full-length PIF1 and PIF1C were purified from overexpressing *E. coli* cells, BL21 (DE3) (31). The strain harboring a plasmid pMStRNA1, in which tRNAs for rare codons were cloned into a R6K derived kanamycin resistant plasmid (32), and pET20b-PIF1 was grown in 3 l of LB supplemented with ampicillin (250 μg/ml) and kanamycine (30 μg/ml) at 15°C, with aeration until the culture reached an A_{600} value of 0.6. Isopropyl β-D-thiogalactopyranoside (IPTG) was added to 0.2 mM, and the incubation was continued for 14 h. The resultant cell paste (9 g) was resuspended in 18 ml of buffer I (50 mM HEPES NaOH pH 7.5, 0.1 mM EDTA, 10 mM β-mercaptoethanol, 1 M NaCl) and frozen in liquid nitrogen. The cells were thawed in ice water and lyzed by addition of 3 ml buffer I containing 100 mM spermidine and 4 mg/ml lysozyme. After incubation on ice for 30 min, heating in a 37°C water bath for 2 min and further incubation on ice for 30 min, the lyzate was clarified by centrifugation twice at 85 000*g* for 30 min at 4°C. Subsequent column chromatography was carried out at 4°C using a fast protein liquid chromatography (FPLC) system (GE Healthcare, Tokyo, Japan). After adding imidazole to 50 mM, the lyzate was applied at 0.2 ml/min to a 1-ml HiTrap chelating column (GE Healthcare), which had been treated with 0.1 M $NiSO_4$ and then equilibrated with buffer A (50 mM HEPES NaOH pH 7.5, 10% glycerol, 10 mM β-mercaptoethanol, 1 M NaCl) containing 50 mM imidazole. The column was washed with 10 ml of equilibration buffer at 0.2 ml/min and his-tagged PIF1 was eluted with 10 ml of buffer A containing 100 mM imidazole. Fractions eluted with 100 mM imidazole were pooled and diluted to 50 mM imidazole with buffer A, then loaded again onto a 1-ml HiTrap chelating column at 0.2 ml/min. The column was washed, and PIF1 was eluted with buffer A containing 300 mM imidazole, then loaded at 0.1 ml/min onto a Superdex 200 10/300 GL column (GE Healthcare) equilibrated with buffer A. PIF1 peak fractions were pooled, frozen in liquid nitrogen, and stored at −80°C. His-tagged PIF1C was purified under the same conditions as described for his-tagged PIF1.

His-tagged human PIF1N was purified from overexpressing *E. coli* cells, Rosetta 2 (DE3) (Novagen, Tokyo, Japan). The strain harboring pET15-PIF1N was grown in 3 l of LB supplemented with ampicillin (250 μg/ml) and chloramphenicol (30 μg/ml) at 15°C with aeration until the culture reached an A_{600} value of 0.6. IPTG was added to 0.2 mM, the incubation was continued for 14 h, and the cells were lyzated as described. After adding imidazole to 50 mM, the lyzate was applied at 0.2 ml/min to a 1-ml HiTrap chelating column, which had been treated with 0.1 M $NiSO_4$ and then equilibrated with buffer A containing 50 mM imidazole. The column was washed with 10 ml of equilibration buffer at 0.2 ml/min and then with 10 ml of buffer A containing 100 mM imidazole. His-tagged PIF1N was eluted with 10 ml of 300 mM imidazole in buffer A. Fractions containing PIF1N were pooled, diluted with buffer B (50 mM HEPES NaOH pH7.5, 10 mM β-mercaptoethanol) to 100 mM of NaCl, and applied at 0.5 ml/min to a 1-ml HiTrap SP HP column (GE Healthcare) equilibrated with buffer B containing 100 mM NaCl. The column was washed with 10 ml of equilibration buffer at 0.1 ml/min, and the PIF1N was eluted with 20 ml of a linear gradient of 100–1000 mM NaCl in buffer B. Fractions containing PIF1N were pooled, frozen in liquid nitrogen and stored at −80°C.

Antibodies

To obtain polyclonal antibodies against PIF1, truncated his-tagged PIF1 proteins (1–180 and 338–641 amino acids) were expressed in Rosetta 2 (DE3), purified and used to immunize rabbits.

DNA substrates

The oligonucleotides employed for the preparation of DNA substrates are listed in Table 1. Oligonucleotides were 5′-end labeled using [γ-^{32}P]ATP (GE Healthcare) and polynucleotide kinase (New England BioLabs, Tokyo, Japan). The schematic structures of substrates are shown in figures, and the labeled oligonucleotides are indicated with asterisks. Annealing reaction mixtures (30 μl) containing the 5′-^{32}P-labeled oligonucleotides at 1 μM, all unlabeled oligonucleotides at 3 μM, 10 mM Tris–HCl (pH 7.5), 7 mM $MgCl_2$ and 200 mM NaCl were heated at 95°C for 10 min, transferred directly to 65°C and held at that temperature for 1 h, slow-cooled to 25°C over a period of 2 h and held at that temperature for 30 min and then cooled to 4°C. Substrates were then purified by electrophoresis through 15–25% polyacrylamide using 0.5× TBE (33) as the electrophoresis buffer. Substrates were eluted from the gel by crushing the gel

slice in TE buffer and incubating overnight at 4°C. The slurry was then filtered through Micro Bio-Spin (Bio-Rad) columns, and the DNA was recovered by ethanol precipitation and resuspended in TE buffer.

ATPase assays

ATPase activity was measured in a standard reaction mixture (20 μl) containing 50 mM Tris–HCl (pH 8.0), 2 mM DTT, 1.2 mM $MgCl_2$, 0.25 mg/ml BSA, 2 mM [γ-^{32}P]ATP, indicated DNA and 1 μl of protein sample diluted with buffer D (50 mM Tris-HCl pH8.0, 1 M NaCl, 2 mM DTT, 10% glycerol, 0.1 mg/ml BSA) to obtain indicated final concentrations. After preincubation for 30 s at 30°C, reactions were initiated by the addition of PIF1 proteins and further incubated for 10 min. After the reaction was stopped with 4 μl of 20 mM EDTA (pH 8.0), an aliquot (2 μl) was spotted onto a polyethyleneimine-cellulose plate (Merck, Tokyo, Japan) and developed in 0.3 M LiCl/0.9 M formic acid. The products were analyzed using a Bio-Imaging Analyzer BAS2000 (Fuji Photo Film Co., Ltd., Tokyo, Japan). The extents of ATP hydrolysis were measured with reference to the relative ratios of radioactivity of inorganic phosphate to uncleaved ATP.

Kinetic assays to determine K_m values for ATP were performed for 10 min in 20 μl reaction mixtures using 14 nM of PIF1 and PIF1C with 3.8 μM and 150 μM (in nucleotides) of M13 mp7 single-stranded (ss) DNA, respectively. Concentrations of ATP ranged from 25 to 400 μM. K_m values were evaluated from the plot of the initial velocity versus the ATP concentration using a hyperbolic curve-fitting program with correlation coefficients (R^2) >0.99.

DNA helicase assays

DNA helicase activity was measured under ATPase assay conditions (20 μl) with the indicated DNA substrate (0.35 nM) and 1 μl of protein sample diluted with buffer D to obtain the indicated final concentrations. After preincubation for 30 s at 30°C, reactions were initiated by the addition of PIF1 proteins and incubated for 10 min at 30°C. Helicase reactions were terminated with 10 μl of stop solution (150 mM EDTA, 30% glycerol, 2% SDS, 0.1% bromophenol blue). In kinetic experiments, a 160-μl reaction mixture was incubated at 30°C and 10-μl aliquots were withdrawn at the indicated times. The reaction products were subjected to electrophoresis through 15–25% polyacrylamide gels in Tris–glycine buffer (33). The gels were dried on DE81 paper (Whatman, Tokyo, Japan) and autoradiographed. DNA products were quantified using a Bio-Imaging Analyzer.

Electrophoretic mobility shift assays

Oligonucleotides were labeled with polynucleotide kinase (New England BioLabs) and [γ-^{32}P]ATP. Assays of DNA binding were performed with a modification of a method described previously (34). The reactions (20 μl) were carried out under ATPase assay conditions, sometimes omitting $MgCl_2$ or ATP, with 25 pM oligonucleotides and 1 μl of protein sample diluted with buffer D to obtain the indicated final concentrations. Incubation was carried out on ice for 10 min followed by loading on prerunning 5% polyacrylamide gels (79:1 acrylamide/*bis*-acrylamide). The electrophoresis buffer contained 6 mM Tris–HCl (pH 8.0), 5 mM sodium acetate and 1 mM EDTA, and the gels were subjected to a constant voltage of 8 V/cm for 100 min at 4°C. Following gel electrophoresis, the products were analyzed as described for the helicase assay. For quantification, fractions of free DNA were measured, and the binding fractions were determined by subtraction from the amount of the free DNA at 0 nM of the protein (35).

For RPA binding experiments, the reactions (20 μl) were carried out under the ATPase assay conditions, sometimes omitting ATP. The substrate 3F:4L (0.35 nM) was incubated, directly or after heating at 100°C for 5 min, with 1 μl of RPA sample diluted with buffer (50 mM HEPES NaOH pH 7.5, 250 mM NaCl, 10 mM β-mercaptoethanol, 10% glycerol) to obtain indicated final concentrations. Incubation was carried out on ice for 10 min, and the products were analyzed as in the PIF1 binding experiments.

DNA strand annealing assays

Strand annealing reactions (20 μl) were carried out under the ATPase assay conditions, but in the presence of the indicated concentrations of ATP, with the 5′-end labeled substrate DNA for helicase assay (0.35 nM), which had been boiled at 100°C for 5 min and quickly chilled on ice before adding to the reaction mixture, and 1 μl of protein sample diluted with buffer D to obtain the indicated final concentrations. After preincubation for 30 s at 30°C, reactions were initiated by the addition of PIF1 proteins, with incubation for 10 min at 30°C. After terminating the reactions with 10 μl of stop solution, the products were analyzed as described for the helicase assay. Kinetic experiments were also carried out as described for the helicase assay.

RESULTS

Purification of PIF1 protein and its deletion derivatives

Previously, biochemical studies of human PIF1 were performed using N-terminal-truncated forms of PIF1 containing only the conserved helicase motifs, located in the C-terminus (Supplementary Figure S2A). However, we found that the PINT domain is well conserved in the PIF1 family (Supplementary Figure S2B), suggesting that it plays a functional role. To examine biochemical activity, we established a procedure to purify full-length PIF1 with a 6× histidine tag at the N-terminus at quantities sufficient for detailed biochemical studies from overproducing *E. coli* cells (Supplementary Figure S2C). We also purified a C-terminal truncated form (PIF1N) and a N-terminal truncated form (PIF1C) (Supplementary Figure S2A) to address biochemical functions of individual domains. PIF1C and PIF1N consist of only the seven helicase motifs and only the PINT domain, respectively (Supplementary Figure S2A and Materials and methods section). Elution profiles from gel filtration chromatography

suggested PIF1 and PIF1C to be monomers (data not shown) as described in yeast homologs (1,5,7). The purified proteins were analyzed by SDS–PAGE followed by CBB staining and western blotting, showing PIF1, PIF1C and PIF1N to have molecular sizes of 71, 54 and 22 kDa, respectively (Supplementary Figure S2C).

Unwinding activities of PIF1 and PIF1C, a mutant lacking PINT domain but containing the helicase domain

We first measured DNA helicase activity of the purified proteins using the indicated DNA substrate (Figure 1A). When 5′ overhang (1F:2S) and 3′ overhang (1R:2S) DNA were used as substrates, we detected helicase activity only on the 5′-overhang substrate, consistent with previous reports (3,9), although the activity was very low (Figure 1B). In the titration experiment, activity was only detected clearly at the maximum concentration of the purified sample (Figure 1B). Since yeast PIF1 homologs preferentially unwind forked structures (1,5,7), we tested a forked substrate (Figure 1C). The titration experiment demonstrated that human PIF1 efficiently unwound the forked substrate with about 10 times higher activity than that for the 5′-overhang substrate (Figure 1C), suggesting that the property was conserved in evolution. Time course experiments using the forked substrate demonstrated that PIF1 could unwind up to 50% of the substrate in a 15 min reaction, although longer incubation did not increase the products (Figure 1D).

To compare the unwinding activity of PIF1C, titration experiments were performed with the forked substrate. We found that PIF1C exhibited helicase activity, but it required more than 100 times more protein to obtain equivalent activity to that of PIF1 (Figure 1C). As a control, we showed that PINT domain itself could not unwind the substrate (Figure 1C). These results suggested that the function of the PINT domain could be enhancement of the unwinding activity of the helicase domain.

Nonstructural ssDNA, but not forked-structural DNA, preferentially stimulates ATPase activity of PIF1

DNA helicases are enzymes with an associated DNA-dependent ATPase activity. They are presumed to use the hydrolysis of ATP to translocate to ssDNA and to subsequently break the hydrogen bonds of duplex DNA. Characterization of ATPase activity could provide important information as a helicase. To analyze ssDNA dependent ATPase activity of PIF1, titration of M13 mp7 ssDNA was performed in reactions with optimal concentrations of ATP and $MgCl_2$ (Figure 2A). The result showed that the ATPase activity was increased depending on the concentrations of ssDNA and reached a plateau between 3 and 50 μM (in nucleotide equivalents) of ssDNA (Figure 2A). The maximum rate of ATP hydrolysis was calculated to be about 1 000 min^{-1}, which was equivalent to 5000 min^{-1} at 37°C of *Sc*Pif1 (5) and 4000 min^{-1} at 30°C of the fission yeast homolog, Pfh1 (7), which have been determined under reaction conditions with nearly saturated concentrations of ssDNA.

To describe precisely the concentration of ssDNA required for ATPase activity, a kinetic parameter,

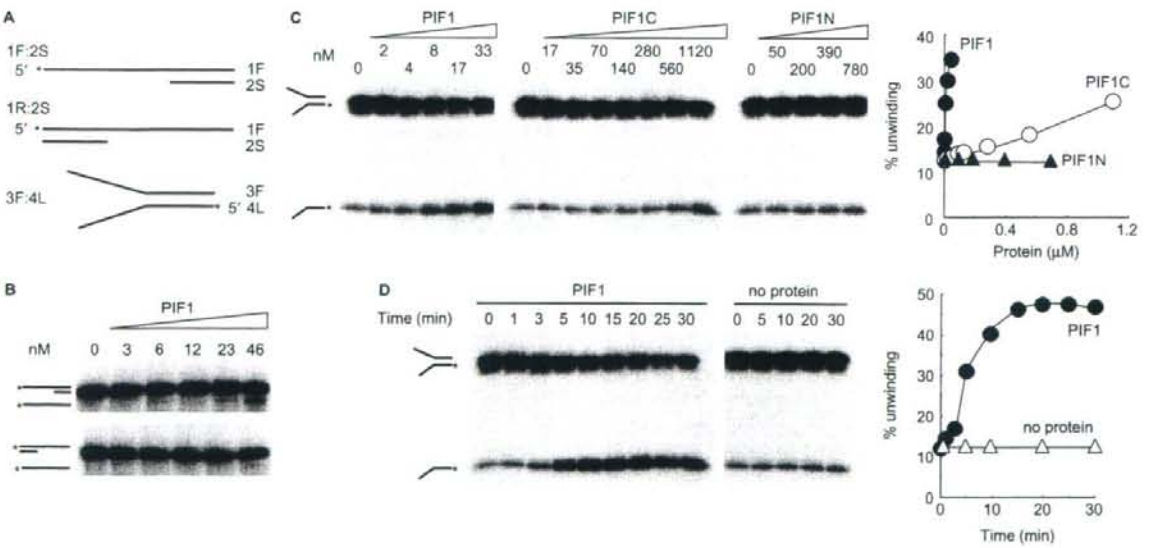

Figure 1. Helicase activity of PIF1. **(A)** Schematic structures of the DNA substrates. The asterisks indicate ^{32}P-labeled 5′ phosphate. **(B)** Helicase activity of PIF1. Increasing levels of PIF1 were incubated with substrates (0.35 nM) with the 5′overhang, 1F:2S (upper panel), or 3′ overhang, 1R:2S (lower panel) under standard reaction mixtures at 30°C for 10 min. Reaction products were separated on a 15–25% polyacrylamide gel. **(C)** Helicase activity of PIF1, PIF1N and PIF1C proteins. The forked structure partial duplex DNA substrate, 3F:4L (0.35 nM), was incubated with the indicated concentrations of PIF1, PIF1N and PIF1C under standard reaction conditions at 30°C for 10 min. The quantified data are shown graphically. The errors in the experiments were <10%. **(D)** Time course of unwinding reactions with PIF1. The forked structure partial duplex DNA substrate, 3F:4L (0.35 nM), was incubated at 30°C for the indicated time under standard reaction conditions with PIF1 (33 nM). The quantified data are shown graphically. The errors in the experiments were <10%.

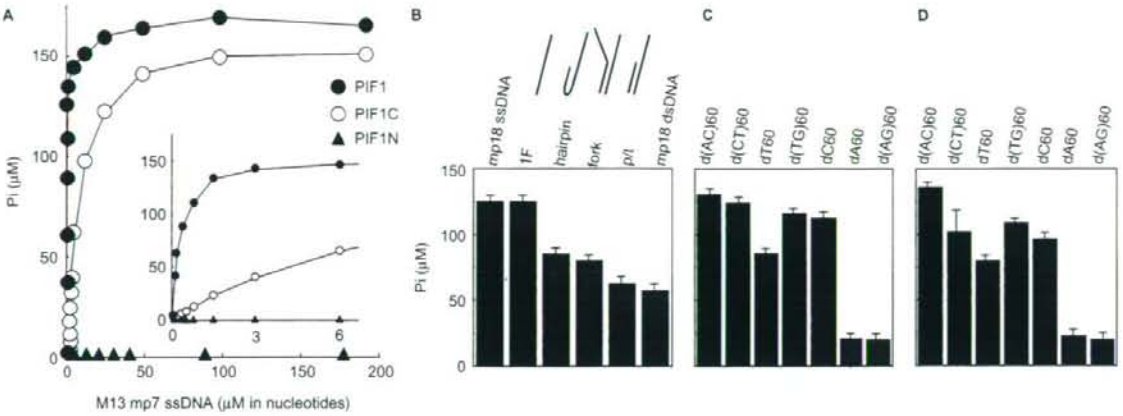

Figure 2. Effects of various DNA molecules on stimulation of ATPase activity of PIF1. **(A)** Titration of M13 mp7 ssDNA for its stimulation of ATPase activity of PIF1, PIF1N and PIF1C. ATPase activities were measured under standard reaction conditions with PIF1 proteins (13.9 nM) at 30°C for 10 min. An aliquot (2 μl) of the reaction products was then analyzed by thin layer chromatography. The extent of ATP hydrolysis was measured by determining the relative radioactivity of the released inorganic phosphate. Inset is a plot of the data at lower concentrations of ss DNA. The errors in the experiments were <10%. **(B)** Effects of the various DNA molecules on stimulation of ATPase activity of PIF1. Assays were performed with the indicated DNA (3.8 μM in nucleotides) and PIF1 (13.9 nM). **(C)** Effects of oligonucleotides with different compositions on stimulation of ATPase activity by PIF1. Assays were performed with indicated DNA (7.5 μM in nucleotides) and PIF1 (14.6 nM). **(D)** Effects of oligonucleotides with different compositions on stimulation of ATPase activity by PIF1C. Assays were performed with indicated DNA (150 μM in nucleotides), and PIF1C (13.9 nM).

K_{eff}, defined as the concentration of ssDNA required to achieve half-maximal ATP hydrolysis (5,36,37) was calculated from the titration curve (Figure 2A) using a hyperbolic curve-fitting program (Table 2). The calculated K_{eff} value, 0.35 μM (in nucleotides) for M13 mp18 ssDNA, agreed with the 0.6 μM (in nucleotides) of *Sc*Pif1 reported for the same M13 ssDNA (5).

Since PIF1 preferentially unwound the forked substrate (Figure 1), we consider that substrate specificity for unwinding activity could be correlated with stimulation of ATPase activity. To seek preferential structures for stimulation for ATPase of PIF1, we tested various DNAs, including a fork-structure, a primer-template-structure, a hairpin-structure and a linear oligonucleotide (Table 1), as well as M13 mp18 ssDNA and double stranded (ds) DNA (Figure 2B). The reactions were carried out with 3.8 μM (in nucleotides) of each oligonucleotide, which was nearly saturated concentration for M13 mp7 ssDNA (Figure 2A inset). Among these, M13 mp18 ssDNA proved to strongly and dsDNA to poorly stimulate ATPase activity (Figure 2B). Moreover, we found surprisingly that a oligonucleotide, 1F, which would not be expected to form secondary structures (Table 1), stimulated ATPase activity to the highest level, equivalent to that of M13 mp18 ssDNA (Figure 2B). The result suggested that an ssDNA region itself, rather than the structure of the DNA, is crucial for stimulation of ATPase activity of PIF1. Consequently, we compared ATPase activity stimulated by seven different 60-mer oligonucleotides composed of one or two nucleotides, guaranteed not to form secondary structures. The reactions were performed in the presence of a nearly saturated concentration of the oligonucleotides (7.5 μM in nucleotides) (Supplementary Figure S3A). The results revealed general features of ssDNA for stimulation of ATPase (Figure 2C), with the order of stimulation being poly(purine–pyrimidine) ≥ polypyrimidine ≫ polypurine.

Since these experiments were performed with nearly saturated concentrations of oligonucleotides, the results do not reflect affinities of the respective ssDNAs. We therefore determined a kinetic parameter, K_{eff}, calculated from data of ssDNA-titration experiments (Supplementary Figure S3A, data not shown) using a hyperbolic curve-fitting program (Table 2). The K_{eff} value for dsDNA was more than 20 times higher than those for ssDNA, showing a preference to ssDNA. For ssDNA, the K_{eff} values, except with polypurine, were essentially the same (~0.1 μM in nucleotides), and slightly lower than with M13 ssDNA and structured DNAs, which was probably due to over estimation of the ssDNA region because of the presence of local double-stranded regions generated by the secondary structure, since the K_{eff} values were expressed in nucleotide equivalents. These results supported our conclusion that the predominant requirement for stimulation of ATPase is nonstructural ssDNA.

Evaluation of ATPase activity of PIF1C, a mutant lacking the PINT domain

We noted that the K_{eff} value for ssDNA of PIF1 was in line with one report for *Sc*Pif1 (5), but significantly lower than that for human PIF1 with a N-terminal truncated form (4). We consider that the difference could be attributed to the missing function of the PINT domain. To test this possibility, we examined ATPase activity of PIF1C (Figure 2A), and also tested PIF1N as a control. First, we confirmed no ATPase activity of PIF1N (Figure 2A),

Table 1. Synthetic oligonucleotides used in this work

Name	Sequence
1F (73-mer)	5′-CTCCTCCTCCTCCTCCTCCTCCTCCTCCTCCTCCTCCTCCTCGCTCGACGCCATTAATAAT GTTTTC-3′
1R (73-mer)	5′-GCTCGACGCCATTAATAATGTTTTCCTCCTCCTCCTCCTCCTCCTCCTCCTCCTCCTCCTCCT CCTC-3′
2L (50-mer)	5′-GAAAACATTATTAATGGCGTCGAGCTAGGCACAAGGCGAACTGCTAACGG-3′
2S (25-mer)	5′-GAAAACATTATTAATGGCGTCGAGC-3′
3F (55-mer)	5′-AGGTCTCGACTAACTCTAGTCGTTGTTCCACCCGTCCACCCGACGCCACCTCCTG-3′
3S (25-mer)	5′-CCCGTCCACCCGACGCCACCTCCTG-3′
4S (25-mer)	5′-CAGGAGGTGGCGTCGGGTGGACGGG-3′
4L (51-mer)	5′-GCAGGAGGTGGCGTCGGGTGGACGGGATTGAAATTTAGGCTGGCACGGTCG-3′
5 (fork) (55-mer)	5′-TTTTTTTTTTTTTTTTTTTTTTTTTTTTTCGGACGCTCGACGCCATTAATAATGTTTTC-3′
7 (fork) (56-mer)	5′-TGAAAACATTATTAATGGCGTCGAGCGTCCGTTTTTTTTTTTTTTTTTTTTTTTT-3′
18 (hairpin) (73-mer)	5′-GCCTGCACGTGGCGATCGTTCGATCGCCACGTGCAGGCGCTGCTGCTGGCTCGACGCCATTAAT AATGTTTTC-3′
90 (p/t) (90-mer)	5′-TGGGCTCACGTGGTCGACGCTGGAGGTGATCACCAGATGATTGCTAGGCATGCTTTCCGCAA GAGAACGGGCGTCTGCGTACCCGTGCAG-3′
30 (p/t) (30-mer)	5′-CTGCACGGGTACGCAGACGCCCGTTCTCTT-3′
d(AC)60 (60-mer)	5′-ACACACACACACACACACACACACACACACACACACACACACACACACACACACAC-3′
d(AG)60 (60-mer)	5′-AGAGAGAGAGAGAGAGAGAGAGAGAGAGAGAGAGAGAGAGAGAGAGAGAGAGAG-3′
d(TG)60 (60-mer)	5′-TGTGTGTGTGTGTGTGTGTGTGTGTGTGTGTGTGTGTGTGTGTGTGTGTGTGTG-3′
d(CT)60 (60-mer)	5′-CTCTCTCTCTCTCTCTCTCTCTCTCTCTCTCTCTCTCTCTCTCTCTCTCTCTCT-3′
d(CT)55 (55-mer)	5′-TCTCTCTCTCTCTCTCTCTCTCTCTCTCTCTCTCTCTCTCTCTCTCT-3′
d(CT)45 (45-mer)	5′-TCTCTCTCTCTCTCTCTCTCTCTCTCTCTCTCTCTCTCT-3′
d(CT)35 (35-mer)	5′-TCTCTCTCTCTCTCTCTCTCTCTCTCTCTCT-3′
d(CT)30 (30-mer)	5′-CTCTCTCTCTCTCTCTCTCTCTCTCT-3′
d(CT)20 (20-mer)	5′-CTCTCTCTCTCTCTCTCT-3′
d(CT)15 (15-mer)	5′-TCTCTCTCTCTCT-3′
dC60 (60-mer)	5′-CCCCCCCCCCCCCCCCCCCCCCCCCCCCCCCCCCCCCCCCCCCCCCCCCCCCCCCCC-3′
dA60 (60-mer)	5′-AAAAAAAAAAAAAAAAAAAAAAAAAAAAAAAAAAAAAAAAAAAAAAAAAAAAAAAAA-3′
dT60 (60-mer)	5′-TTTTTTTTTTTTTTTTTTTTTTTTTTTTTTTTTTTTTTTTTTTTTTTTTTTTTTTTT-3′

Table 2. Kinetic parameters for the ATPase activity of PIF1 with various ssDNAs

DNA	PIF1 K_{eff}[a] (μM)	PIF1C K_{eff} (μM)
M13 mp7 ssDNA	0.35	8.7
M13 mp18 ssDNA	0.45	–[b]
M13 mp18 dsDNA	9.7	–
1F[c]	0.17	–
hairpin (18)[c]	0.71	–
fork (5:7)[c]	0.39	–
p/t (90:30)[c]	0.80	–
d(AC)60[c]	0.13	3.7
d(CT)60[c]	0.11	2.3
d(TG)30[c]	0.12	3.4
dT60[c]	0.11	6.4
dC60[c]	0.07	2.3
dA60[c]	1.2	nd[d]
d(AG)60[c]	1.8	nd

Kinetic assays to determine K_{eff} values were performed for 10 min in 20 μl reaction mixtures using 14 nM of PIF1 and PIF1C. Concentrations of ssDNA ranged from 0.15 to 300 μM in nucleotides. K_{eff} values were evaluated from the plot of the initial velocity versus the nucleotide concentration using a hyperbolic curve-fitting program with the correlation coefficients (R^2) more than 0.97, which were shown in supplementary Figure S3.

[a]K_{eff} is expressed in nucleotides equivalents.

[b]Not determined.

[c]Nucleotide sequences were shown in Table 1.

[d]Not detected.

as expected from the lack of any ATPase motifs. When M13 mp7 ssDNA was titrated in the reaction with PIF1C, we detected similar levels of maximum ATPase activity at higher concentrations of ssDNA (Figure 2A), suggesting that the helicase domain is sufficient to express ATPase activity. However, the required concentrations of ssDNA to achieve maximal activity were significantly increased (Figure 2A inset). The calculated K_{eff} value, 8.7 μM (in nucleotides) for M13 mp7 ssDNAs with PIF1C was more than 20 times higher than that for PIF1 (Table 2). This property was also demonstrated by determining K_{eff} values for different oligonucleotides (Table 2), calculated from data from ssDNA titration experiments (Supplementary Figure S3B). These results suggested that a defect in PIF1C could be in the binding to ssDNA, and the PINT domain could help interaction between the helicase domain and ssDNA.

To determine preferential nucleotide compositions for PIF1C stimulation of ATPase activity, it was measured using the same set of the oligonucleotides in the reactions with nearly saturated concentrations of the oligonucleotides (150 μM in nucleotides) (Supplementary Figure S3B). The results demonstrated that the preference of PIF1C was essentially identical to that of PIF1 (Figure 2C and D), suggesting that it is intrinsic to the helicase domain, the PINT domain not affecting this property.

For further comparison between PIF1 and PIF1C, we determined their K_m values for ATP in the reactions with saturating concentrations of M13 mp18 ssDNA, 3.8 and 150 μM (in nucleotides), respectively. The K_m values for ATP of both proteins were both 0.17 mM and essentially identical to the previously reported value of 0.2 mM for N-terminal-truncated human PIF1 (4). This result

suggested again that the helicase domain is sufficient to express ssDNA-dependent ATPase activity.

Characterization of ssDNA binding activities of PIF1 and PIF1C

It seemed that the apparent affinity to ssDNA for the helicase domain (PIF1C) was much lower than that for PIF1 in ATPase reactions. We considered that the defect might be attributed to binding ability to ssDNA. To measure DNA binding of PIF1 and PIF1C directly, we performed electrophoretic mobility shift assays (EMSA) using a oligonucleotide, d(AC)60 (Table 1) as a model substrate. It has been reported that this assay detects DNA–protein complexes in yeast and human PIF1 in an ATP-independent manner (7,9). Binding reactions were carried out under the optimal ATPase assay conditions, then products were loaded on gels as described in the Materials and methods section. The titration experiment displayed PIF1–DNA complexes, which were increased depending on the concentration of PIF1 (Figure 3A). The apparent K_d, which is approximately equal to the protein concentration at which half the free DNA has become bound (35), was determined to be about 3 nM. This was in good agreement with the K_{eff} value of d(AC)60 for ATPase activity, because the 0.13 μM (in nucleotides) (Table 2) corrected for the concentration of the 60-mer oligonucleotide became 2 nM.

When PIF1C was tested, we could detect PIF1C–DNA complexes, but the affinity seemed much lower than that with PIF1, demonstrating a defect in ssDNA binding activity. When the point at which half the free DNA has become bound was extrapolated from the binding curve, the apparent K_d value was estimated at about 10 nM. However, the K_d value was not directly correlated with the K_{eff} value, since it was still 6 times lower than the

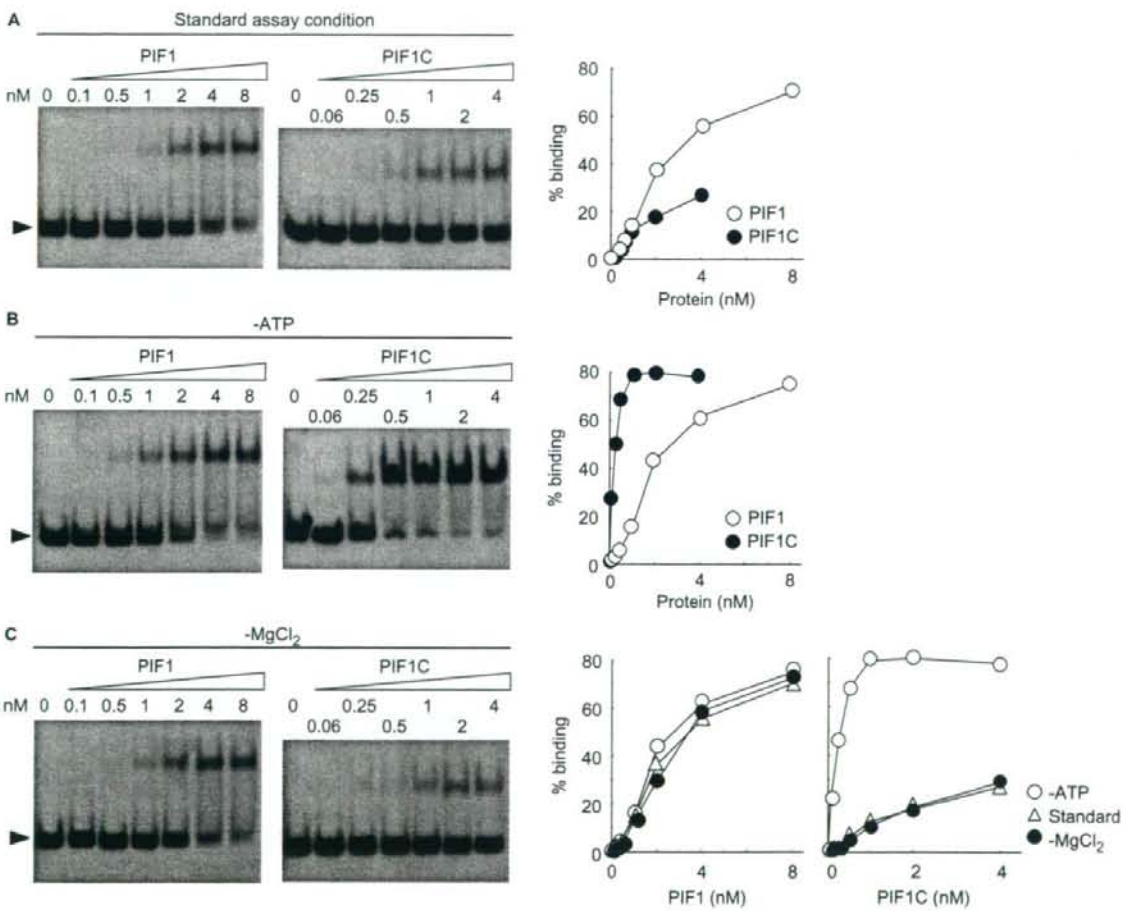

Figure 3. EMSA of PIF1 and PIF1C for binding to ssDNA. (**A**) EMSA of ssDNA binding to PIF1 and PIF1C under standard reaction conditions. The 5′-^{32}P labeled oligonucleotide, d(AC)60, was incubated with the indicated concentrations of PIF1. Arrowheads indicate the positions of free DNA. The quantified data are shown graphically. (**B**) EMSA in the absence of ATP. Experiments were performed as described in (A). The quantified data are shown graphically. (**C**) EMSA in the absence of $MgCl_2$. Experiments were performed as described in (A). The quantified data are shown graphically together with data from (A) and (B). The errors in the experiments were <10%.

apparent K_{eff} value of 60 nM (in oligonucleotides), with the K_{eff} value of 3.7 μM (in nucleotides) (Table 2), corrected for the concentration of the 60-mer oligonucleotide.

Since it was very likely that ATP could influence the binding reaction, we performed the same experiments without ATP. With the full length PIF1, the titration curve was not affected (Figure 3B). In contrast that for PIF1C in the absence of ATP was significantly changed. The apparent affinity was increased to about 0.3 nM (Figure 3B). To determine whether the effect of ATP is caused by binding or hydrolysis, titration experiments were carried out omitting $MgCl_2$ to prevent hydrolysis of ATP (Figure 3C). Under this condition, the ATPase activity was under the background level (data not shown), suggesting that, even though trace amounts of Mg ions were present as contaminants of chemicals, the contribution was negligible. The result clearly demonstrated the binding curves to be identical to that under standard assay conditions containing ATP and $MgCl_2$ (Figure 3C), suggesting that ATP binding itself affected the interaction between ssDNA and the helicase domain.

ssDNA binding activity of the PIF1N

Our results suggested that the PINT domain plays a role in modulating the ssDNA binding activity of the helicase domain. Therefore, we carried out the same binding assays with PIF1N (Figure 4A). The assays detected PIF1N–DNA complexes, and the titration curves were not affected by ATP and $MgCl_2$ (Figure 4A), with an apparent K_d value of about 10 nM. These results suggested that PIF1N itself possesses ATP-independent ssDNA binding activity.

In contrast to the binding reactions with PIF1 and PIF1C shown in Figure 3, further shifts of the mobility

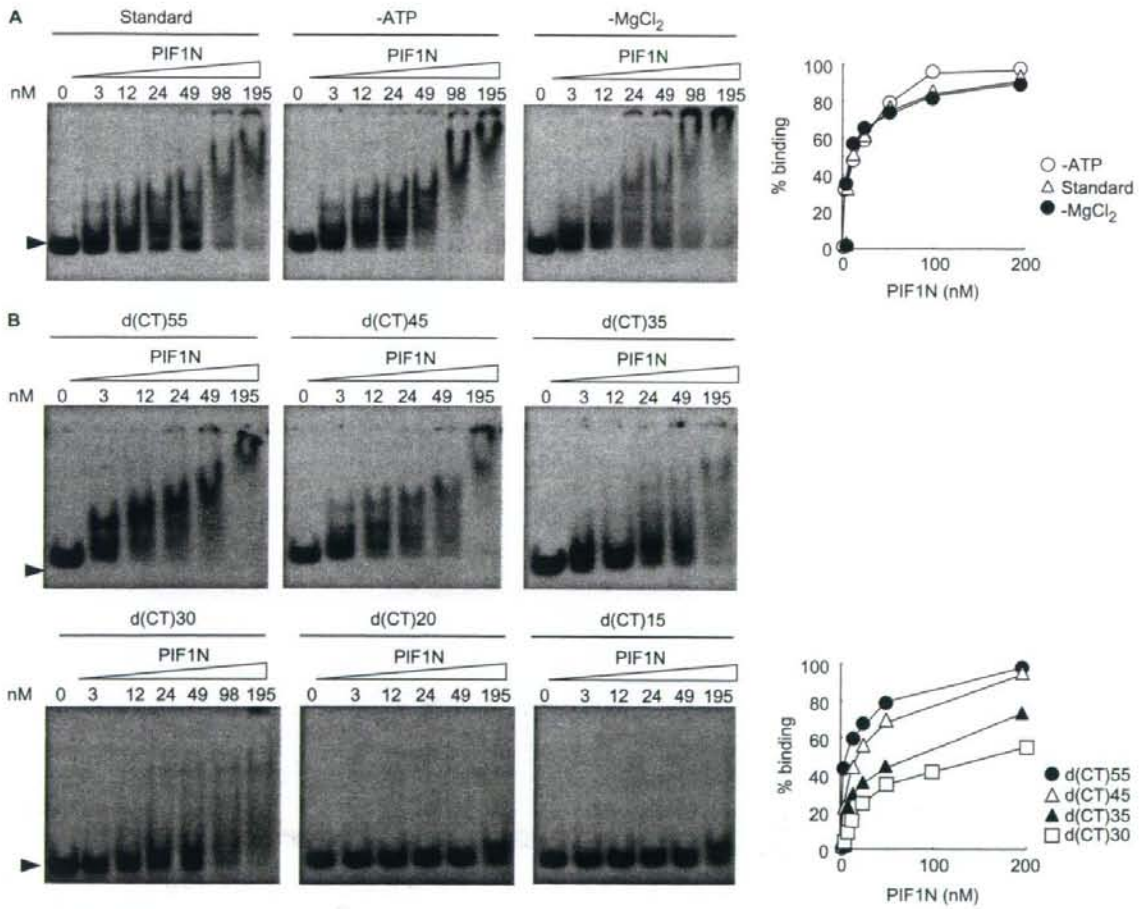

Figure 4. EMSA of PIF1N for binding to ssDNA. **(A)** Titration of PIF1N under different conditions. The 5′-^{32}P labeled oligonucleotide, d(AC)60, was incubated with the shown concentrations of PIF1N, omitting ATP or $MgCl_2$ as indicated. Arrowheads indicate the positions of free DNA. The quantified data are shown graphically. **(B)** Binding ability of PIF1N to different sizes of oligonucleotides. Experiments were performed using indicated oligonucleotides as substrates under standard reaction conditions in the absence of ATP. The quantified data are shown graphically. The errors in the experiments were <10%.

of the complexes with PIF1N in higher concentrations were observed (Figure 4A). This could be due to more than one protein molecule binding to the 60-mer oligonucleotide. To determine the minimal ssDNA size for binding of PIF1N, six different oligonucleotides in lengths ranging from 55 to 15 bases were subjected to binding assays. When the 55-mer was used as the substrate, the result was essentially identical to that for a 60-mer. However, further reduction of the length to 45-mer and 35-mer decreased the extent of multiple binding. With the 30-mer oligonucleotide, but not the 20-mer and 15-mer, a distinct band of the complex was observed. These results demonstrated that the minimal ssDNA size could be between 30 and 20 bases.

DNA strand annealing activity of PIF1, residing in the PINT domain

During helicase assays, we unexpectedly found that PIF1 possessed robust annealing activity. For detailed analysis, a forked substrate (1F:2L) (Figure 5A) was denatured by heating at 100°C for 5 min, and then incubated with PIF1 under the conditions for the standard ATPase assay omitting ATP to avoid unwinding reactions. Titration of PIF1 showed about 50% of ssDNA could be annealed within 10 min when 46 nM PIF1 was present (Figure 5B). To determine the region of PIF1 responsible for the annealing activity, PIF1C and PIF1N were tested for their ability to promote the reaction. The results demonstrated that PIF1N, but not PIF1C, efficiently annealed ssDNA, with activity only 3-fold lower than that of PIF1 when 1F and 2L substrates were tested (Figure 5B). This result indicated that the annealing activity of PIF1 resides in the PINT domain.

Since ATP is essential for helicase activity, we tested effects of ATP on the annealing reaction. To avoid the effect of unwinding, titration of ATP was carried out in the absence of $MgCl_2$. The result demonstrated both PIF1 and PIF1N to be inhibited by ATP (Figure 5C). Time course experiments demonstrated that, in the absence of ATP, PIF1 annealed up to 70% of ssDNA, whereas, in the presence of the optimal concentration of ATP (2 mM) for helicase activity, the annealed fraction reached only 20% (Figure 5D). The properties of PIF1 were same as those of PIF1N, 2 mM ATP also inhibiting annealing activity from 50% to 17% (Figure 5E). Importantly, the ATP-titration curve and time course with PIF1 were essentially identical to those for PIF1N (Figure 5C–E), suggesting that the properties are intrinsic to the PINT domain.

Further confirming this conclusion, we used completely complementary strands as a substrate. The annealing product has no ssDNA region, preventing product unwinding under the standard reaction conditions containing ATP and $MgCl_2$. Titration curves of ATP for PIF1 and PIF1N demonstrated again inhibitory effects, although significant fractions of the substrates were spontaneously annealed under the assay conditions (Figure 5F).

Effects of RPA on unwinding and annealing reactions of PIF1

Elucidation of whether PIF1 has the potential to promote unwinding and annealing reactions on RPA-coated substrates is valuable for understanding cellular functions of PIF1. To do this, first, we determined the optimal concentration of RPA for the substrate DNA binding by EMSA. The substrate, 3F:4L was used for the binding reactions at the final concentration of 0.35 nM. The results of titration of RPA are shown in Figure 6A. When the concentration of RPA was increased to 0.9 nM, one molecule of RPA bound to at least one strand of the forked substrate. At >1.8 nM, each strand of the substrate was probably occupied by one RPA molecule (Figure 6A). The levels of apparent affinity of RPA for ssDNA were in good agreement with previous reports (38).

Then we examined unwinding activity of PIF1. RPA was mixed with the forked substrate, 3F:4L, under the standard reaction conditions on ice, then PIF1 was introduced and incubation was performed at 30°C for 10 min. We found that RPA did not affect unwinding reactions at low concentrations <0.4 nM (Figure 6B, left panel), in which majority of the substrate was RPA-free (Figure 6A). When the concentration of RPA reached 0.9 nM, at which almost all the oligonucleotides were occupied with RPA (Figure 6A), severe inhibition was observed (Figure 6B, left panel). At much higher concentrations of RPA, we observed unwinding products (Figure 6B, left panel). However, a control experiment without PIF1 revealed that the products detected at higher concentrations >1.8 nM of RPA were PIF1 independent (Figure 6B, right panel). The quantified results shown in Figure 6C demonstrate no difference in the two reactions at higher concentrations of RPA (>0.9 nM). These results suggest that RPA does not enhance, but rather inhibits, the helicase activity of PIF1.

To examine annealing activity in the presence of RPA, we also determined the optimal concentration of RPA for ssDNA binding. In the reactions, we used the same substrate as for the unwinding assay (3F:4L) at the final concentration of 0.35 nM, but after denaturation by heating. The assay detected only complexes with the labeled oligonucleotide 3F (55-mer), although another fragment, 4L (51-mer), was present. The results of titration of RPA are shown in Figure 6D. When the concentration of RPA was increased to 0.9 nM, almost all the oligonucleotides 3F and probably 4L were occupied by at least one molecule of RPA. At >1.8 nM, the oligonucleotides were occupied by two molecules of RPA (Figure 6D).

Next, we carried out annealing assays under the same conditions. RPA was mixed with heat denatured substrate (3F and 4L) on ice, then PIF1 was introduced with incubation at 30°C for 10 min. The result clearly demonstrated an inhibitory effect of RPA (Figure 6E). The quantified results for inhibition of annealing reactions well correlated inversely with the amount of RPA binding (Figure 6F).

DISCUSSION

In this article, we document for the first time the biochemical properties of full-length human PIF1 together with those of truncated forms consisting of individual domains. We could establish intrinsic properties of the helicase domain and functional roles of the PINT domain.

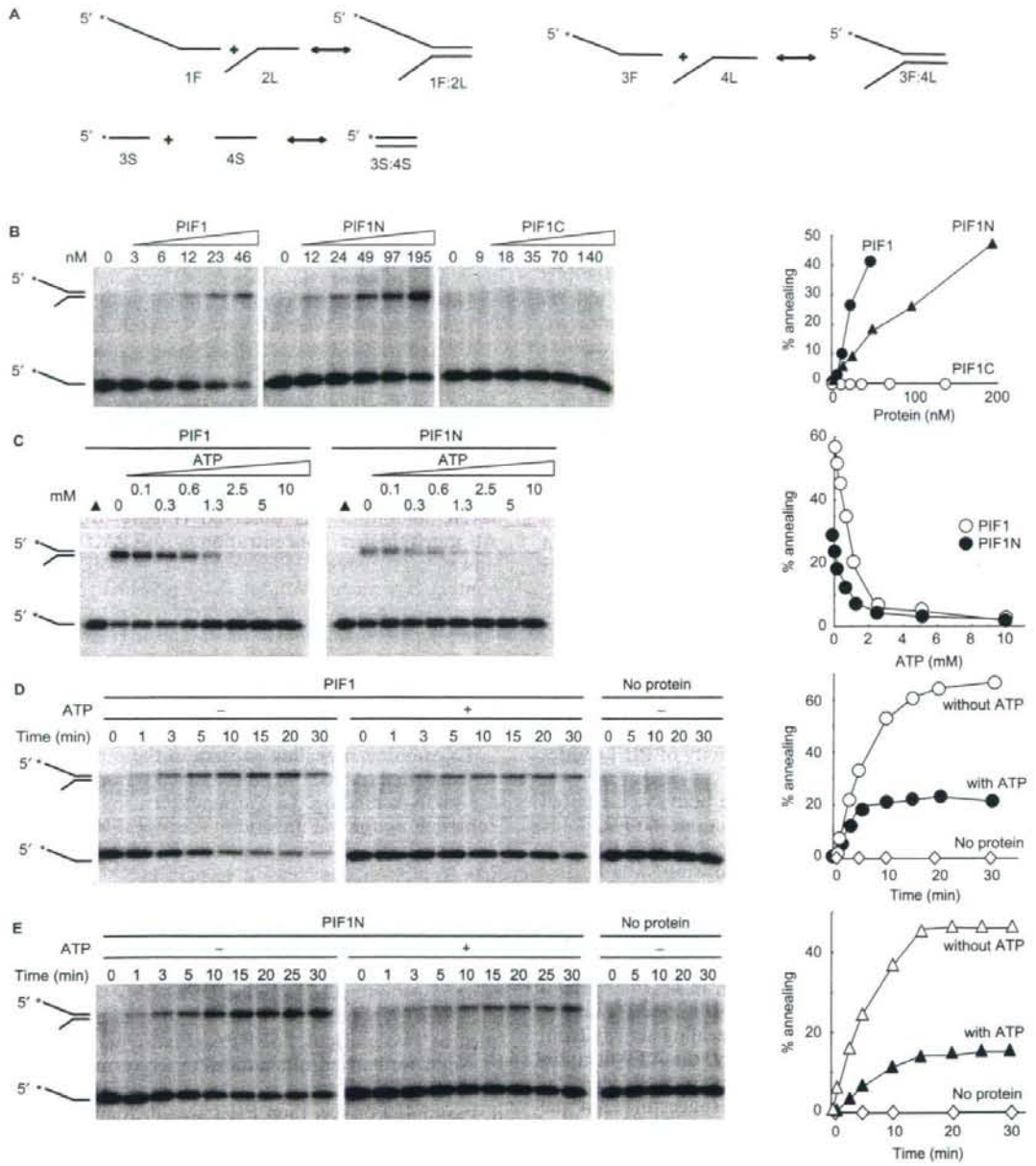

Figure 5. DNA strand annealing activity. (**A**) Schematic structures of the DNA substrates. The asterisks indicate ^{32}P-labeled 5′-phosphate. (**B**) Annealing activities of PIF1, PIF1C and PIF1N. The fork-structural partial duplex DNA substrate, 1F:2L (0.35 nM), was boiled for 5 min, then incubated with increasing levels of PIF1, PIF1C and PIF1N as indicated under standard reaction conditions omitting ATP at 30°C for 10 min. The quantified data are shown graphically. (**C**) Titration of ATP on annealing reactions mediated by PIF1 and PIF1N. The fork-structural partial duplex DNA substrate, 3F:4L (0.35 nM), was boiled for 5 min, then incubated with PIF1 (33 nM) or PIF1N (195 nM) and increasing levels of ATP under standard reaction conditions omitting $MgCl_2$ at 30°C for 10 min. The quantified data are shown graphically. (**D**) Time course of annealing reactions mediated by PIF1 under standard reaction conditions omitting $MgCl_2$. Heat denatured substrate DNA, 1F:2L (0.35 nM), was incubated with PIF1 (46 nM). The quantified data are shown graphically. (**E**) Time course of annealing reactions mediated by PIF1N under standard reaction conditions omitting $MgCl_2$. Heat denatured substrate DNA, 1F:2L (0.35 nM), was incubated with PIF1N (195 nM). The quantified data are shown graphically. (**F**) Titration of ATP on annealing reactions mediated by PIF1 and PIF1N under standard reaction conditions. A complete double stranded oligonucleotide, 3S:4S (0.35 nM) was boiled for 5 min, then incubated with PIF1 (30 nM) or PIF1N (195 nM) and increasing levels of ATP under standard reaction conditions at 30°C for 10 min. The quantified data are shown graphically. The errors in the experiments were <10%.